Probing new physics in semileptonic Λ_b decays

Atasi Ray,[1,*] Suchismita Sahoo,[2,†] and Rukmani Mohanta[1,‡]
[1]School of Physics, University of Hyderabad, Hyderabad 500046, India
[2]Theoretical Physics Division, Physical Research Laboratory, Ahmedabad 380009, India

(Received 25 September 2018; published 7 January 2019)

In recent times, several hints of lepton nonuniversality have been observed in semileptonic B meson decays, both in the charged-current ($b \to c l \bar{\nu}_l$) and neutral-current ($b \to s l l$) transitions. Motivated by these intriguing results, we perform a model-independent analysis of the semileptonic Λ_b decays involving the quark level transitions $b \to (u, c) l \nu_l$, in order to scrutinize the nature of new physics. We constrain the new parameter space by using the measured branching ratios of the $B_{c,u}^+ \to \tau^+ \nu_\tau$, $B \to \pi \tau \nu_\tau$ processes and the existing experimental results on the $R_{D^{(*)}}$, $R_{J/\psi}$, and R_π^l parameters. Using the constrained parameters, we estimate the branching ratios, forward-backward asymmetries, and hadron and lepton polarization asymmetries of the $\Lambda_b \to (\Lambda_c, p) l \nu_l$ processes. Moreover, we also examine whether there could be any lepton universality violation in these decay modes.

DOI: 10.1103/PhysRevD.99.015015

I. INTRODUCTION

Though the Standard Model (SM) is considered as the most fundamental theory describing almost all the phenomena of particle physics, still it is unable to shed light on some of the open issues, like matter-antimatter asymmetry, dark matter, dark energy, etc., which eventually necessitates probing the physics beyond it. In this respect, the rare decays of B mesons involving the flavor changing neutral current (FCNC) transitions play an important role in the quest for new physics (NP). Even though the SM gauge interactions are lepton flavor universal, the violation of lepton universality has been observed in various semileptonic B decays. Recently, the LHCb Collaboration has reported a spectacular discrepancy of 1.9σ (3.3σ) [1–6] and 2σ [7] on the lepton nonuniversality (LNU) parameters $R_{D^{(*)}} = \mathrm{Br}(\bar{B} \to \bar{D}^{(*)} \tau \bar{\nu}_\tau)/\mathrm{Br}(\bar{B} \to \bar{D}^{(*)} l \bar{\nu}_l)$ and $R_{J/\psi} = \mathrm{Br}(B_c \to J/\psi \tau \bar{\nu}_\tau)/\mathrm{Br}(B_c \to J/\psi l \bar{\nu}_l)$, respectively, from their corresponding SM values. Analogous LNU parameters are also observed in $b \to s l l$ processes, i.e., $R_{K^{(*)}} = \mathrm{Br}(\bar{B} \to \bar{K}^{(*)} \mu^+ \mu^-)/\mathrm{Br}(\bar{B} \to \bar{K}^{(*)} e^+ e^-)$ with discrepancies of 2.6σ $(2.2 - 2.4)\sigma$ [8,9]. The SM predictions, as well as the corresponding experimental values of various LNU parameters, along with their deviations, are presented in Table I.

In addition, another discrepancy in the $b \to u l \bar{\nu}_l$ transition is also noticed in the measured ratio

$$R_\pi^l = \frac{\tau_{B^0}}{\tau_{B^-}} \frac{\mathrm{Br}(B^- \to \tau^- \bar{\nu}_\tau)}{\mathrm{Br}(B^0 \to \pi^+ l^- \bar{\nu}_l)}, \quad l = e, \mu, \tag{1}$$

where $\tau_{B^0}(\tau_{B^-})$ is the lifetime of the $B^0(B^-)$ meson. Using the experimental measured values of the branching ratios of the $B_u^- \to \tau^- \bar{\nu}_\tau$ and $B^0 \to \pi^+ l^- \bar{\nu}_l$ decay processes

$$\mathrm{Br}(B_u^- \to \tau^- \bar{\nu}_\tau)|^{\mathrm{Expt}} = (1.09 \pm 0.24) \times 10^{-4}, \tag{2}$$

$$\mathrm{Br}(B^0 \to \pi^+ l^- \bar{\nu}_l)|^{\mathrm{Expt}} = (1.45 \pm 0.05) \times 10^{-4}, \tag{3}$$

with $\tau_{B^-}/\tau_{B^0} = 1.076 \pm 0.004$ from [17], one can obtain

$$R_\pi^l|^{\mathrm{Expt}} = 0.699 \pm 0.156, \tag{4}$$

which has also nearly 1σ deviation from its SM value $R_\pi^l|^{\mathrm{SM}} = 0.583 \pm 0.055$. It is generally argued that, compared to the first two generations, the processes involving the third generation leptons are more sensitive to NP due to their reasonably large mass. As the LNU parameters are the ratio of branching fractions, the uncertainties arising due to the CKM matrix elements and hadronic form factors are expected to be reduced, as they are canceled out in the ratio. Hence, these deviations of various LNU parameters hint towards the possible interplay of new physics in an ambiguous manner.

On the other hand, around 20% of the total number of hadrons produced at LHCb are Λ_b baryons [18,19], and

*atasiray92@gmail.com
†suchismita8792@gmail.com
‡rmsp@uohyd.ernet.in

TABLE I. List of measured lepton nonuniversality parameters.

LNU parameters	Experimental value	SM prediction	Deviation
$R_K\vert_{q^2\in[1,6]\ \mathrm{GeV}^2}$	$0.745^{+0.090}_{-0.074} \pm 0.036$ [8]	1.003 ± 0.0001 [10]	2.6σ
$R_{K^*}\vert_{q^2\in[0.045,1.1]\ \mathrm{GeV}^2}$	$0.66^{+0.11}_{-0.07} \pm 0.03$ [9]	0.92 ± 0.02 [11]	2.2σ
$R_{K^*}\vert_{q^2\in[1.1,6]\ \mathrm{GeV}^2}$	$0.69^{+0.11}_{-0.07} \pm 0.05$ [9]	1.00 ± 0.01 [11]	2.4σ
R_D	$0.391 \pm 0.041 \pm 0.028$ [6]	0.300 ± 0.008 [12]	1.9σ
R_{D^*}	$0.316 \pm 0.016 \pm 0.010$ [6]	0.252 ± 0.003 [13,14]	3.3σ
$R_{J/\psi}$	$0.71 \pm 0.17 \pm 0.184$ [7]	0.289 ± 0.01 [15,16]	2σ

hence the study of Λ_b becomes quite interesting in these days. The $b \to q l \bar{\nu}_l (q = u, c)$ quark level transitions can be probed in both B and Λ_b decays. Thus, as in B decays one can also scrutinize the presence of the lepton universality violation in the corresponding semileptonic baryon decays $\Lambda_b \to (\Lambda_c, p) l \bar{\nu}_l$ to corroborate the results from the B sector and, thus, to probe the structure of NP. The heavy-heavy and heavy-light semileptonic decays of baryons can serve as an additional source for the determination of the Cabibbo-Kobayashi-Maskawa (CKM) matrix elements V_{qb} [17,20–22]. In the literature [23–35], the baryonic decay modes mediated by $b \to (u, c) l \bar{\nu}_l$ quark level transitions have been studied both in model-dependent and model-independent approaches. The analysis of $\Lambda_b \to \Lambda_c \tau \bar{\nu}_\tau$ decay in the context of SM and various NP couplings was performed in [25]. In Ref. [27], the SM hadron and lepton polarization asymmetries were computed in the covariant confined quark model. The precise lattice QCD calculation of $\Lambda_b \to (\Lambda_c, p)$ form factors and the investigation of semileptonic baryonic $b \to (u, c) l \bar{\nu}_l$ processes were performed in [28]. The authors of Ref. [34] investigated the impact of five possible new physics interactions, adopting five different form factors of the $\Lambda_b \to \Lambda_c \tau \bar{\nu}_\tau$ decay mode. Considering various real NP couplings, the differential decay distributions, forward-backward asymmetries, and ratios of the branching fractions of these baryonic decay modes were investigated in [29]. In this work, we intend to analyze the effect of complex new couplings on the $\Lambda_b \to (\Lambda_c, p) l \bar{\nu}_l$ decay processes in a model-independent way. The main goal of this work is to check the possible existence of the lepton universality violation in baryonic decays. The new coefficients are constrained by using the branching ratios of the $B_{u,c} \to \tau \bar{\nu}_\tau$, $B \to \pi \tau \bar{\nu}_\tau$ processes and the experimental data on the $R_{D^{(*)}}$, $R_{J/\psi}$, R_π^l ratios. We then compute the branching ratios, forward-backward asymmetries, and lepton and hadron polarization asymmetries of these baryonic decay modes. We also check the LNU parameters by using the constrained new couplings. The main difference between our approach and the previous analyses in [25,32] is that we investigate the impact of individual complex new couplings on all the angular observables, including the lepton and hadron polarization asymmetries. We use the updated experimental limits on $R_{D^{(*)}}$, R_π^l ratios, including the new $R_{J/\psi}$ parameter to constrain the allowed parameter space.

The outline of our paper is follows. In Sec. II, we present the general effective Lagrangian of $b \to (u, c) l \nu_l$ processes in the presence of NP and the necessary theoretical framework for analyzing these processes. The constraints on a new parameter space associated with $b \to (u, c) l \bar{\nu}_l$ transitions are computed from the experimental data on $R_{D^{(*)}}$, $R_{J/\psi}$, R_π^l, $\mathrm{Br}(B_{c,u} \to \tau \bar{\nu}_\tau)$, and $\mathrm{Br}(B \to \pi \tau \bar{\nu}_\tau)$ observables in Sec. III. In Sec. IV, we discuss the branching ratios and all the physical angular observables of $\Lambda_b \to (\Lambda_c, p) l \bar{\nu}_l$ processes. Our findings are summarized in Sec. V.

II. THEORETICAL FRAMEWORK

The most general effective Lagrangian associated with $B_1 \to B_2 l \bar{\nu}_l$ decay processes, where $B_1 = \Lambda_b$, $B_2 = \Lambda_c$, p mediated by the quark level transition $b \to q l \bar{\nu}_l (q = u, c)$ is given by [36,37]

$$\mathcal{L}_{\mathrm{eff}} = -\frac{4G_F}{\sqrt{2}} V_{qb} \{ (1 + V_L) \bar{l}_L \gamma_\mu \nu_L \bar{q}_L \gamma^\mu b_L + V_R \bar{l}_L \gamma_\mu \nu_L \bar{q}_R \gamma^\mu b_R + S_L \bar{l}_R \nu_L \bar{q}_R b_L + S_R \bar{l}_R \nu_L \bar{q}_L b_R + T_L \bar{l}_R \sigma_{\mu\nu} \nu_L \bar{q}_R \sigma^{\mu\nu} b_L \} + \mathrm{H.c.}, \tag{5}$$

where G_F denotes the Fermi constant, V_{qb} are the CKM matrix elements, and $q(l)_{L,R} = P_{L,R} q(l)$ are the chiral quark (lepton) fields with $P_{L,R} = (1 \mp \gamma_5)/2$ as the projection operators. Here $V_{L,R}$, $S_{L,R}$, T_L represent the vector-, scalar-, and tensor-type NP couplings, which are zero in the SM.

In the presence of NP, the double differential decay distribution for $B_1 \to B_2 l \bar{\nu}_l$ processes with respect to q^2 and $\cos\theta_l$ (θ_l is the angle between the directions of the parent B_1 baryon and the l^- in the dilepton rest frame) is given as [25,33]

$$\frac{d\Gamma}{dq^2} = N\left(1-\frac{m_l^2}{q^2}\right)^2\left[A_1+\frac{m_l^2}{q^2}A_2+2A_3+\frac{1}{4}A_4+\frac{4m_l}{\sqrt{q^2}}(A_5+A_6)+A_7\right], \tag{6}$$

where

$$\begin{aligned}
A_1 &= 2\sin^2\theta_l(H^2_{\frac{1}{2},0}+H^2_{-\frac{1}{2},0})+(1-\cos\theta_l)^2H^2_{\frac{1}{2},+}+(1+\cos\theta_l)^2H^2_{-\frac{1}{2},-},\\
A_2 &= 2\cos^2\theta_l(H^2_{\frac{1}{2},0}+H^2_{-\frac{1}{2},0})+\sin^2\theta_l(H^2_{\frac{1}{2},+}+H^2_{-\frac{1}{2},-})+2(H^2_{\frac{1}{2},t}+H^2_{-\frac{1}{2},t})-4\cos\theta_l(H_{\frac{1}{2},0}H_{\frac{1}{2},t}+H_{-\frac{1}{2},0}H_{-\frac{1}{2},t}),\\
A_3 &= H^{SP^2}_{\frac{1}{2},0}+H^{SP^2}_{-\frac{1}{2},0},\\
A_4 &= \frac{m_l^2}{q^2}[2\sin^2\theta_l(H^{T^2}_{\frac{1}{2},+,-}+H^{T^2}_{\frac{1}{2},0,t}+H^{T^2}_{-\frac{1}{2},+,-}+H^{T^2}_{-\frac{1}{2},0,t}+2H^{T}_{\frac{1}{2},+,-}H^{T}_{\frac{1}{2},0,t}+2H^{T}_{-\frac{1}{2},+,-}H^{T}_{-\frac{1}{2},0,t})+(1+\cos\theta_l)^2(H^{T^2}_{-\frac{1}{2},0,-}+H^{T^2}_{-\frac{1}{2},-,t}\\
&\quad+2H^{T}_{-\frac{1}{2},0,-}H^{T}_{-\frac{1}{2},-,t})+(1-\cos\theta_l)^2(H^{T^2}_{\frac{1}{2},+,0}+H^{T^2}_{\frac{1}{2},+,t}+2H^{T}_{\frac{1}{2},+,0}H^{T}_{\frac{1}{2},+,t})]+2\cos^2\theta_l(H^{T^2}_{\frac{1}{2},+,-}+H^{T^2}_{\frac{1}{2},0,t}+H^{T^2}_{-\frac{1}{2},+,-}+H^{T^2}_{-\frac{1}{2},0,t}\\
&\quad+2H^{T}_{\frac{1}{2},+,-}H^{T}_{\frac{1}{2},0,t}+2H^{T}_{-\frac{1}{2},+,-}H^{T}_{-\frac{1}{2},0,t})+\sin^2\theta_l(H^{T2}_{\frac{1}{2},+,0}+H^{T^2}_{\frac{1}{2},+,t}+H^{T2}_{-\frac{1}{2},0,-}+H^{T^2}_{-\frac{1}{2},-,t}+2H^{T}_{\frac{1}{2},+,0}H^{T}_{\frac{1}{2},+,t}+2H^{T}_{-\frac{1}{2},0,-}H^{T}_{-\frac{1}{2},-,t}),\\
A_5 &= -\cos\theta_\ell(H_{\frac{1}{2},0}H^{SP}_{\frac{1}{2},0}+H_{-\frac{1}{2},0}H^{SP}_{-\frac{1}{2},0})+(H_{\frac{1}{2},t}H^{SP}_{\frac{1}{2},0}+H_{-\frac{1}{2},t}H^{SP}_{-\frac{1}{2},0}),\\
A_6 &= \frac{\cos^2\theta_l}{2}(H_{\frac{1}{2},0}H^{T}_{\frac{1}{2},+,-}+H_{\frac{1}{2},0}H^{T}_{\frac{1}{2},0,t}+H_{-\frac{1}{2},0}H^{T}_{-\frac{1}{2},+,-}+H_{-\frac{1}{2},0}H^{T}_{-\frac{1}{2},0,t})-\frac{\cos\theta_l}{2}(H_{\frac{1}{2},t}H^{T}_{\frac{1}{2},+,-}+H_{\frac{1}{2},t}H^{T}_{\frac{1}{2},0,t}+H_{-\frac{1}{2},t}H^{T}_{-\frac{1}{2},+,-}\\
&\quad+H_{-\frac{1}{2},t}H^{T}_{-\frac{1}{2},0,t})+\frac{(1-\cos\theta_l)^2}{4}(H_{\frac{1}{2},+}H^{T}_{\frac{1}{2},+,0}+H_{\frac{1}{2},+}H^{T}_{\frac{1}{2},+,t})+\frac{(1+\cos\theta_l)^2}{4}(H_{-\frac{1}{2},-}H^{T}_{-\frac{1}{2},0,-}+H_{-\frac{1}{2},-}H^{T}_{-\frac{1}{2},-,t})\\
&\quad+\frac{\sin^2\theta_l}{4}(H_{\frac{1}{2},+}H^{T}_{\frac{1}{2},+,0}+H_{\frac{1}{2},+}H^{T}_{\frac{1}{2},+,t}+H_{-\frac{1}{2},-}H^{T}_{-\frac{1}{2},0,-}+H_{-\frac{1}{2},-}H^{T}_{-\frac{1}{2},-,t}\\
&\quad+2H_{\frac{1}{2},0}H^{T}_{\frac{1}{2},+,-}+2H_{\frac{1}{2},0}H^{T}_{\frac{1}{2},0,t}+2H_{-\frac{1}{2},0}H^{T}_{-\frac{1}{2},+,-}+2H_{-\frac{1}{2},0}H^{T}_{-\frac{1}{2},0,t}),\\
A_7 &= -2\cos\theta_l(H^{SP}_{\frac{1}{2},0}H^{T}_{\frac{1}{2},+,-}+H^{SP}_{\frac{1}{2},0}H^{T}_{\frac{1}{2},0,t}+H^{SP}_{-\frac{1}{2},0}H^{T}_{-\frac{1}{2},+,-}+H^{SP}_{-\frac{1}{2},0}H^{T}_{-\frac{1}{2},0,t}),
\end{aligned} \tag{7}$$

with

$$\begin{aligned}
H^{VA}_{\lambda_{\Lambda_c},\lambda} &= H^{V}_{\lambda_{\Lambda_c},\lambda}-H^{A}_{\lambda_{\Lambda_c},\lambda}, \qquad H^{V}_{\lambda_{\Lambda_c},\lambda_w}=H^{V}_{-\lambda_{\Lambda_c},-\lambda_w}, \qquad H^{A}_{\lambda_{\Lambda_c},\lambda_w}=-H^{A}_{-\lambda_{\Lambda_c},-\lambda_w},\\
H^{SP}_{\lambda_{\Lambda_c},\lambda=0} &= H^{S}_{\lambda_{\Lambda_c},\lambda=0}+H^{P}_{\lambda_{\Lambda_c},\lambda=0}, \qquad H^{S}_{\lambda_{\Lambda_c},\lambda_{NP}}=H^{S}_{-\lambda_{\Lambda_c},-\lambda_{NP}}, \qquad H^{P}_{\lambda_{\Lambda_c},\lambda_{NP}}=-H^{P}_{-\lambda_{\Lambda_c},-\lambda_{NP}},\\
H^{T}_{\lambda_{\Lambda_c},\lambda,\lambda'} &= -H^{T}_{\lambda_{\Lambda_c},\lambda',\lambda}, \qquad H^{T}_{\lambda_{\Lambda_c},\lambda,\lambda}=0
\end{aligned} \tag{8}$$

and

$$N = \frac{G_F^2|V_{qb}|^2q^2\sqrt{\lambda(M_{B_1}^2,M_{B_2}^2,q^2)}}{2^{10}\pi^3M_{B_1}^3}, \quad \lambda(a,b,c)=a^2+b^2+c^2-2(ab+bc+ca). \tag{9}$$

Here $M_{B_{1(2)}}$ and m_l are the masses of the $B_{1(2)}$ baryons and charged leptons, respectively. The helicity amplitudes in terms of the various form factors and the NP couplings are given as [25,33]

$$
\begin{aligned}
H^V_{\frac{1}{2}0} &= (1+V_L+V_R)\frac{\sqrt{Q_-}}{\sqrt{q^2}}[(M_{B_1}+M_{B_2})f_1(q^2)-q^2 f_2(q^2)],\\
H^A_{\frac{1}{2}0} &= (1+V_L-V_R)\frac{\sqrt{Q_+}}{\sqrt{q^2}}[(M_{B_1}-M_{B_2})g_1(q^2)+q^2 g_2(q^2)],\\
H^V_{\frac{1}{2}+} &= (1+V_L+V_R)\sqrt{2Q_-}[-f_1(q^2)+(M_{B_1}+M_{B_2})f_2(q^2)],\\
H^A_{\frac{1}{2}+} &= (1+V_L-V_R)\sqrt{2Q_+}[-g_1(q^2)-(M_{B_1}-M_{B_2})g_2(q^2)],\\
H^V_{\frac{1}{2}t} &= (1+V_L+V_R)\frac{\sqrt{Q_+}}{\sqrt{q^2}}[(M_{B_1}-M_{B_2})f_1(q^2)+q^2 f_3(q^2)],\\
H^A_{\frac{1}{2}t} &= (1+V_L-V_R)\frac{\sqrt{Q_-}}{\sqrt{q^2}}[(M_{B_1}+M_{B_2})g_1(q^2)-q^2 g_3(q^2)],\\
H^S_{\frac{1}{2}0} &= (S_L+S_R)\frac{\sqrt{Q_+}}{m_b-m_q}[(M_{B_1}-M_{B_2})f_1(q^2)+q^2 f_3(q^2)],\\
H^P_{\frac{1}{2}0} &= (S_L-S_R)\frac{\sqrt{Q_-}}{m_b+m_q}[(M_{B_1}+M_{B_2})g_1(q^2)-q^2 g_3(q^2)],\\
H^T_{\frac{1}{2},+,0} &= -T_L\sqrt{\frac{2}{q^2}}(f_T\sqrt{Q_+}(M_{B_1}-M_{B_2})+g_T\sqrt{Q_-}(M_{B_1}+M_{B_2})),\\
H^T_{\frac{1}{2},+,-} &= -T_L(f_T\sqrt{Q_+}+g_T\sqrt{Q_-}),\\
H^T_{\frac{1}{2},+,t} &= T_L\left[-\sqrt{\frac{2}{q^2}}(f_T\sqrt{Q_-}(M_{B_1}+M_{B_2})+g_T\sqrt{Q_+}(M_{B_1}-M_{B_2}))+\sqrt{2q^2}(f_T^V\sqrt{Q_-}-g_T^V\sqrt{Q_+})\right],\\
H^T_{\frac{1}{2},0,t} &= T_L[-f_T\sqrt{Q_-}-g_T\sqrt{Q_+}+f_T^V\sqrt{Q_-}(M_{B_1}+M_{B_2})-g_T^V\sqrt{Q_+}(M_{B_1}-M_{B_2})+f_T^S\sqrt{Q_-}Q_++g_T^S\sqrt{Q_+}Q_-],\\
H^T_{-\frac{1}{2},+,-} &= T_L[f_T\sqrt{Q_+}-g_T\sqrt{Q_-}],\\
H^T_{-\frac{1}{2},0,-} &= T_L\left[\sqrt{\frac{2}{q^2}}(f_T\sqrt{Q_+}(M_{B_1}-M_{B_2})-g_T\sqrt{Q_-}(M_{B_1}+M_{B_2}))\right],\\
H^T_{-\frac{1}{2},-,t} &= T_L\left[-\sqrt{\frac{2}{q^2}}(f_T\sqrt{Q_-}(M_{B_1}+M_{B_2})-g_T\sqrt{Q_+}(M_{B_1}-M_{B_2}))+\sqrt{2q^2}(f_T^V\sqrt{Q_-}+g_T^V\sqrt{Q_+})\right],\\
H^T_{-\frac{1}{2},0,t} &= T_L[-f_T\sqrt{Q_-}+g_T\sqrt{Q_+}+f_T^V\sqrt{Q_-}(M_{B_1}+M_{B_2})+g_T^V\sqrt{Q_+}(M_{B_1}-M_{B_2})+f_T^S\sqrt{Q_-}Q_+-g_T^S\sqrt{Q_+}Q_-],
\end{aligned}
\tag{10}
$$

where $Q_\pm=(M_{B_1}\pm M_{B_2})^2-q^2$ and $f_i^{(a)}$, $g_i^{(b)}$ ($i=1,2,3,T$ and $a,b=V,S$) are the various form factors. After integrating out $\cos\theta_l$ in Eq. (6), one can obtain the q^2-dependent differential decay rate. Besides the branching ratios, other interesting observables in these decay modes are

(i) Forward-backward asymmetry parameter:

$$
A_{\rm FB}(q^2)=\left(\int_{-1}^{0}d\cos\theta_l\frac{d^2\Gamma}{dq^2 d\cos\theta_l}-\int_{0}^{1}d\cos\theta_l\frac{d^2\Gamma}{dq^2 d\cos\theta_l}\right)\Big/\frac{d\Gamma}{dq^2}. \tag{11}
$$

(ii) Convexity parameter:

$$
C_F^l(q^2)=\frac{1}{d\Gamma/dq^2}\frac{d^2}{d(\cos\theta_l)^2}\left(\frac{d^2\Gamma}{dq^2 d\cos\theta_l}\right). \tag{12}
$$

(iii) Longitudinal hadron polarization asymmetry parameter:

$$
P_L^h(q^2)=\frac{d\Gamma^{\lambda_2=1/2}/dq^2-d\Gamma^{\lambda_2=-1/2}/dq^2}{d\Gamma/dq^2}, \tag{13}
$$

where $d\Gamma^{\lambda_2=\pm1/2}$ are the individual helicity-dependent differential decay rates, whose detailed expressions are given in Appendix A [33].

(iv) Longitudinal lepton polarization asymmetry parameter:

$$P_L^{\tau}(q^2) = \frac{d\Gamma^{\lambda_\tau=1/2}/dq^2 - d\Gamma^{\lambda_\tau=-1/2}/dq^2}{d\Gamma/dq^2}, \quad (14)$$

where $d\Gamma^{\lambda_2=\pm 1/2}$ are the individual helicity-dependent differential decay rates, whose detailed expressions are given in Appendix A [33].

(v) Lepton nonuniversality parameter:

$$R_{B_2} = \frac{\mathrm{Br}(B_1 \to B_2 \tau^- \bar{\nu}_\tau)}{\mathrm{Br}(B_1 \to B_2 l^- \bar{\nu}_l)}, \quad l = e, \mu. \quad (15)$$

(vi) The LHCb Collaboration has measured the ratio of the partially integrated decay rates of $\Lambda_b^0 \to p\mu\bar{\nu}_l$ over the $\Lambda_b^0 \to \Lambda_c^+ \mu \bar{\nu}_l$ process as

$$R^{\mu}_{\Lambda_c p} = \int_{15\ \mathrm{GeV}^2}^{q^2_{\max}} \frac{d\Gamma(\Lambda_b \to p\mu\bar{\nu}_l)}{dq^2} dq^2 \Big/ \int_{7\ \mathrm{GeV}^2}^{q^2_{\max}} \frac{d\Gamma(\Lambda_b \to \Lambda_c \mu \bar{\nu}_l)}{dq^2} dq^2 = (1.00 \pm 0.04 \pm 0.08) \times 10^{-2} \quad (16)$$

and put constraints on the ratio $|V_{ub}|/|V_{cb}| = 0.083 \pm 0.004 \pm 0.004$ [20]. Similarly, we define the following parameter, to investigate if there is any possible role of NP:

$$R^{\tau}_{\Lambda_c p} = \int_{15\ \mathrm{GeV}^2}^{q^2_{\max}} \frac{d\Gamma(\Lambda_b \to p\tau\bar{\nu}_\tau)}{dq^2} dq^2 \Big/ \int_{7\ \mathrm{GeV}^2}^{q^2_{\max}} \frac{d\Gamma(\Lambda_b \to \Lambda_c \tau \bar{\nu}_\tau)}{dq^2} dq^2. \quad (17)$$

III. CONSTRAINTS ON NEW COUPLINGS

After assembling the expressions for all the interesting observables in the presence of NP, we now proceed to constrain the new coefficients by using the experimental bounds on the $\mathrm{Br}(B_{u,c} \to \tau\bar{\nu}_\tau)$, $\mathrm{Br}(B \to \pi\tau\bar{\nu}_\tau)$, R_π^l, $R_{D^{(*)}}$, and $R_{J/\psi}$ parameters. In this analysis, the new Wilson coefficients are considered as complex. We further assume that only one new coefficient is present at a time and accordingly compute the allowed parameter space of these couplings.

The branching ratios of the $B_q \to l\bar{\nu}_l$ processes in the presence of NP couplings are given by [38]

$$\mathrm{Br}(B_q \to l\bar{\nu}_l) = \frac{G_F^2 |V_{qb}|^2}{8\pi} \tau_{B_q} f_{B_q}^2 m_l^2 M_{B_q} \left(1 - \frac{m_l^2}{M_{B_q}^2}\right)^2 \times \left| (1 + V_L - V_R) - \frac{M_{B_q}^2}{m_l (m_b + m_q)} (S_L - S_R) \right|^2, \quad (18)$$

where M_{B_q} is the mass of the B_q meson. By using the masses of all the particles; the lifetime of the B_q meson; CKM matrix elements from [17]; and decay constants $f_{B_u} = 190.5 \pm 4.2$ MeV, $f_{B_c} = 489 \pm 4 \pm 3$ MeV from [39,40], the branching ratios of the $B_{u,c}^+ \to \tau^+ \nu_\tau$ processes in the SM are found to be

$$\mathrm{Br}(B_u^+ \to \tau^+ \nu_\tau)|^{\mathrm{SM}} = (8.48 \pm 0.5) \times 10^{-5}, \quad (19)$$

$$\mathrm{Br}(B_c^+ \to \tau^+ \nu_\tau)|^{\mathrm{SM}} = (3.6 \pm 0.14) \times 10^{-2}. \quad (20)$$

Using the current world average of the B_c lifetime, the upper limit on the branching ratio of the $B_c^+ \to \tau^+ \nu_\tau$ process is [41]

$$\mathrm{Br}(B_c^+ \to \tau^+ \nu_\tau) \lesssim 30\%. \quad (21)$$

The branching ratios of $B_q \to P l \bar{\nu}_l$ ($P = \pi, D$) are given as [42,43]

$$\frac{d\mathrm{Br}(B_q \to P l \bar{\nu}_l)}{dq^2} = \tau_{B_q} \frac{G_F^2 |V_{qb}|^2}{192\pi^3 M_{B_q}^3} q^2 \sqrt{\lambda(M_{B_q}^2, M_P^2, q^2)} \left(1 - \frac{m_l^2}{q^2}\right)^2 \left\{ |1 + V_L + V_R|^2 \left[\left(1 + \frac{m_l^2}{2q^2}\right) H_0^2 + \frac{3}{2} \frac{m_l^2}{q^2} H_t^2 \right] + \frac{3}{2} |S_L + S_R|^2 H_S^2 + 8 |T_L|^2 \left(1 + \frac{2m_l^2}{q^2}\right) H_T^2 + 3\mathrm{Re}[(1 + V_L + V_R)(S_L^* + S_R^*)] \frac{m_l}{\sqrt{q^2}} H_S H_t - 12\mathrm{Re}[(1 + V_L + V_R) T_L^*] \frac{m_l}{\sqrt{q^2}} H_T H_0 \right\}, \quad (22)$$

where the helicity amplitudes in terms of the form factors ($F_{0,+}$) are expressed as

$$H_0=\sqrt{\frac{\lambda(M_{B_q}^2,M_P^2,q^2)}{q^2}}F_+(q^2),\quad H_t=\frac{M_{B_q}^2-M_P^2}{\sqrt{q^2}}F_0(q^2),$$
$$H_S=\frac{M_{B_q}^2-M_P^2}{m_b-m_q}F_0(q^2)\quad H_T=-\frac{\sqrt{\lambda(M_{B_q}^2,M_P^2,q^2)}}{M_{B_q}+M_P}F_T(q^2). \tag{23}$$

Using the values of the $B\to\pi$ form factors from [44–47], the obtained branching ratios of the $B_q\to\pi l\nu_l$ processes in the SM are given as

$$\mathrm{Br}(B^0\to\pi^+\mu^-\bar{\nu}_\mu)|^{\mathrm{SM}}=(1.35\pm0.10)\times10^{-4}, \tag{24}$$

$$\mathrm{Br}(B^0\to\pi^+\tau^-\bar{\nu}_\tau)|^{\mathrm{SM}}=(9.40\pm0.75)\times10^{-5}. \tag{25}$$

It should be noted that the branching ratio of the muonic channel agrees reasonably well with the experimental value as given in Eq. (3), whereas the tau channel is within its current experimental limit [17],

$$\mathrm{Br}(B^0\to\pi^+\tau^-\bar{\nu}_\tau)|^{\mathrm{Expt}}<2.5\times10^{-4}. \tag{26}$$

The branching ratios of $B_q\to Vl\bar{\nu}_l$, where $V=D^*,J/\psi$, are given as [42,43]

$$\begin{aligned}\frac{d\mathrm{Br}(\bar{B}_q\to Vl\bar{\nu}_l)}{dq^2}&=\tau_{B_q}\frac{G_F^2|V_{qb}|^2}{192\pi^3M_{B_q}^3}q^2\sqrt{\lambda(M_{B_q}^2,M_V^2,q^2)}\left(1-\frac{m_l^2}{q^2}\right)^2\Big\{(|1+V_L|^2+|V_R|^2)\Big[\left(1+\frac{m_l^2}{2q^2}\right)(H_{V,+}^2+H_{V,-}^2+H_{V,0}^2)\\&+\frac{3}{2}\frac{m_l^2}{q^2}H_{V,t}^2\Big]-2\mathrm{Re}[(1+V_L)V_R^*]\Big[\left(1+\frac{m_l^2}{2q^2}\right)(H_{V,0}^2+2H_{V,+}H_{V,-})+\frac{3}{2}\frac{m_l^2}{q^2}H_{V,t}^2\Big]\\&+\frac{3}{2}|S_L-S_R|^2H_S^2+8|T_L|^2\left(1+\frac{2m_l^2}{q^2}\right)(H_{T,+}^2+H_{T,-}^2+H_{T,0}^2)+3\mathrm{Re}[(1+V_L-V_R)(S_L^*-S_R^*)]\\&\times\frac{m_l}{\sqrt{q^2}}H_SH_{V,t}-12\mathrm{Re}[(1+V_L)T_L^*]\frac{m_l}{\sqrt{q^2}}(H_{T,0}H_{V,0}+H_{T,+}H_{V,+}-H_{T,-}H_{V,-})\\&+12\mathrm{Re}[V_RT_L^*]\frac{m_l}{\sqrt{q^2}}(H_{T,0}H_{V,0}+H_{T,+}H_{V,-}-H_{T,-}H_{V,+})\Big\},\end{aligned} \tag{27}$$

where $H_{V,\pm}$, $H_{V,0}$, $H_{V,t}$, and H_S are the hadronic amplitudes [42,43].

In this analysis, we consider the new physics contribution to the third generation lepton only and the couplings with light leptons are assumed to be SM-like. By allowing only one coefficient at a time, we constrain its real and imaginary parts by comparing the theoretically predicted values of $\mathrm{Br}(B_u^+\to\tau^+\nu_\tau)$ and R_π^l with their corresponding 3σ range of observed experimental results for $b\to u\tau\bar{\nu}_\tau$ transitions. We have also used the upper limit of the branching ratio of the $B^0\to\pi^+\tau^-\bar{\nu}_\tau$ process. In Fig. 1, we show the constraints on real and imaginary parts of new coefficients V_L (top left panel), V_R (top right panel), S_L (middle left panel), and S_R (middle right panel) obtained from the $\mathrm{Br}(B_u^+\to\tau^+\nu_\tau)$, $\mathrm{Br}(B^0\to\pi^+\tau^-\bar{\nu}_\tau)$, and R_π^l observables. Since the branching ratio of the $B_u^+\to\tau^+\nu_\tau$ process does not receive any contribution from the tensor operator, the allowed region of the real and imaginary parts of the tensor coupling (T_L) is obtained only from the upper limit on $\mathrm{Br}(B^0\to\pi^+\tau^-\bar{\nu}_\tau)$ and is presented in the bottom panel of this figure. Now imposing the extrema conditions, the allowed range of the new couplings associated with the $b\to u\tau\bar{\nu}_\tau$ transition is presented in Table II. For the case of the $b\to c\tau\bar{\nu}_\tau$ decay processes, the constraints on the real and imaginary parts of individual V_L (top left panel), V_R (top right panel), S_L (middle left panel), and S_R (middle right panel) coefficients obtained from $R_{D^{(*)}}$ and $R_{J/\psi}$ parameters are shown in Fig. 2. Till now, there has been no precise determination of the form factors associated with tensorial operators for the $B_c\to J/\psi l\bar{\nu}_l$ process both from the theoretical and experimental sides. In addition, the leptonic B_c meson decays do not receive any contribution from tensor coupling. Therefore, the constraints on T_L coupling are obtained from the experimental data on $R_{D^{(*)}}$, which is shown in the bottom panel of Fig. 2. In Table II, we have presented the allowed values of $(\mathrm{Re}[V_{L(R)}]-\mathrm{Im}[V_{L(R)}])$ and $(\mathrm{Re}[S_{L(R)}]-\mathrm{Im}[S_{L(R)}])$ coefficients, which are compatible with the 3σ range of the experimental data.

The constraints on these parameters are obtained earlier from various B decays in Refs. [13,14,25,29,38,43,48–50]. Our analysis is similar to Refs. [25,32]. In Ref. [25], the authors have considered the couplings to be complex and constrained the new coefficients associated with $b\to c\tau\bar{\nu}_\tau$ from $R_{D^{(*)}}$ data. However, they have not included the tensor couplings in their analysis and found that the effects produced by the pseudoscalar coefficient are larger than those obtained from the scalar coefficient. In Ref. [29], the author assumed the couplings as real and computed the allowed parameter space by comparing the $R_{D^{(*)}}$, R_π^l

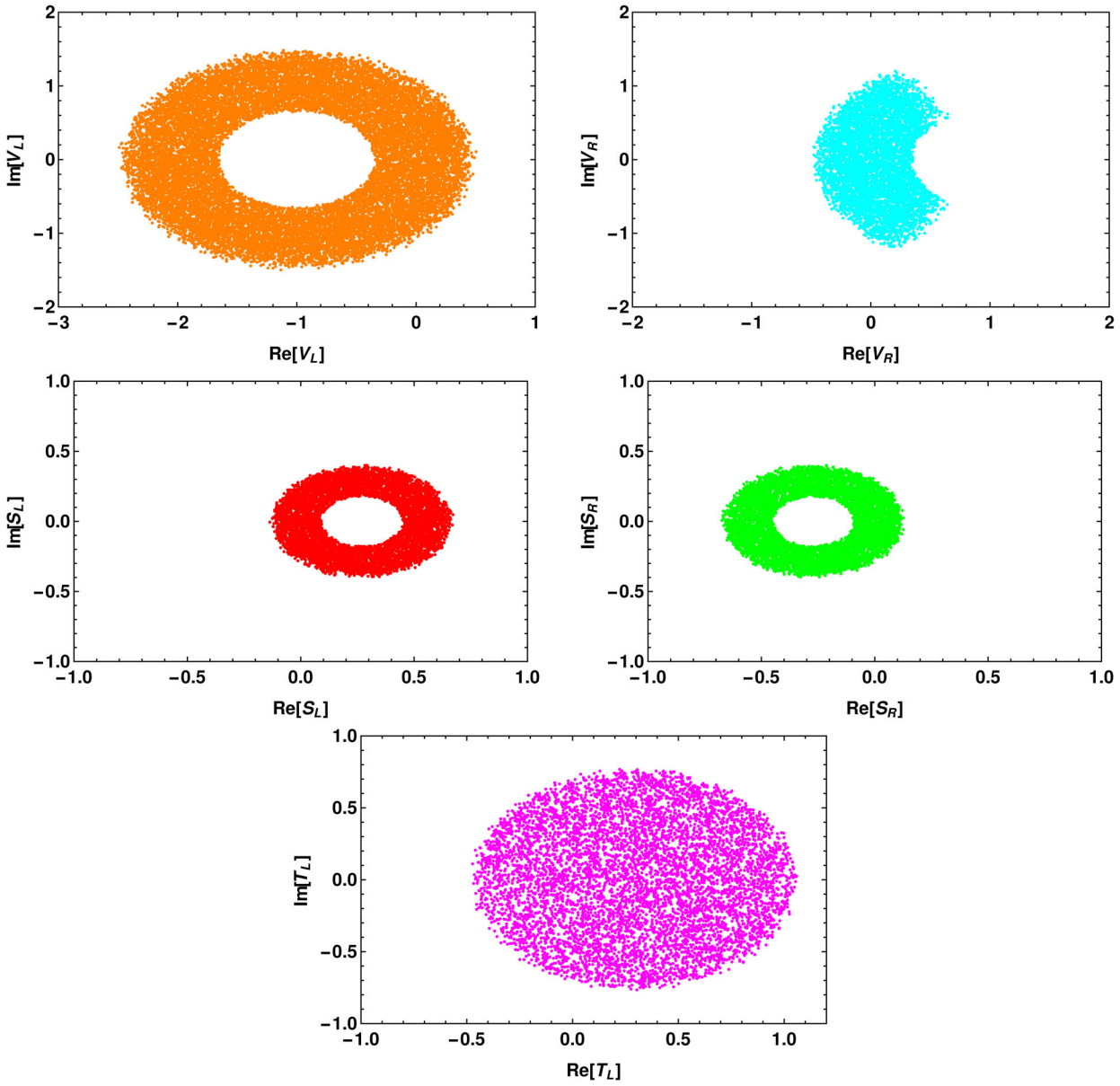

FIG. 1. Constraints on V_L (top left panel), V_R (top right panel), S_L (middle left panel), S_R (middle right panel), and T_L (bottom panel) coefficients associated with the $b \to u\tau\bar{\nu}_\tau$ transitions, obtained from the $\mathrm{Br}(\mathrm{B}_\mathrm{u}^+ \to \tau^+\nu_\tau)$, $\mathrm{Br}(\mathrm{B} \to \pi\tau\bar{\nu}_\tau)$, and R_π^l observables. Here the constraint on the T_L coupling is obtained from $\mathrm{Br}(\mathrm{B} \to \pi\tau\bar{\nu}_\tau)$ experimental data.

parameters with their corresponding 3σ experimental data. In [50], the authors have considered the covariant confined quark model and studied the effect of new physics in the $\bar{B}^0 \to D^*\tau^-\bar{\nu}_\tau$. They took the new coefficients as complex and constrained them using the experimental values of R_D and R_{D^*} within their 2σ range. Recently, the decay process $B_c \to (J/\psi)\tau\nu_\tau$ has been studied, in the covariant confined quark model [49], where the parameter space is constrained by using the experimental values of R_D, R_{D^*}, and $R_{J/\psi}$ within 2σ range. The new coefficients are considered to be complex and their best-fit values are $V_L = -1.05 + i1.15$, $V_R = 0.04 + i0.60$, and $T_L = 0.38 - i0.06$. Though our analysis is similar to these approaches, we get more severe bounds on the phases and strengths of the couplings due to additional constraints from the $\mathrm{Br}(B_c \to \tau\nu_\tau)$ and $R_{J/\psi}$ parameters for the $b \to c\tau\bar{\nu}_\tau$ case and from the $\mathrm{Br}(B_u \to \tau\nu_\tau)$ and $\mathrm{Br}(B \to \pi\tau\nu_\tau)$ observables for the $b \to u\tau\bar{\nu}_\tau$ process.

IV. NUMERICAL ANALYSIS AND DISCUSSION

In this section, we present the numerical results for semileptonic Λ_b decay modes with third generation leptons in the final state. The masses of all the particles and the lifetime of Λ_b are taken from [17]. The q^2 dependence of the helicity form factors ($f_{+,\perp,0}$, $g_{+,\perp,0}$, $h_{+,\perp}$, $\tilde{h}_{+,\perp}$) in the lattice QCD calculation can be parametrized as [28,32]

TABLE II. Allowed ranges of the new coefficients.

Decay processes	New coefficients	Minimum value	Maximum value
$b \to u\tau\bar{\nu}_\tau$	$(\mathrm{Re}[V_L], \mathrm{Im}[V_L])$	$(-2.489, -1.5)$	$(0.504, 1.48)$
	$(\mathrm{Re}[V_R], \mathrm{Im}[V_R])$	$(-0.478, -1.185)$	$(0.645, 1.198)$
	$(\mathrm{Re}[S_L], \mathrm{Im}[S_L])$	$(-0.136, -0.396)$	$(0.672, 0.398)$
	$(\mathrm{Re}[S_R], \mathrm{Im}[S_R])$	$(-0.6743, -0.398)$	$(0.1265, 0.398)$
	$(\mathrm{Re}[T_L], \mathrm{Im}[T_L])$	$(-0.473, -0.773)$	$(1.07, 0.773)$
$b \to c\tau\bar{\nu}_\tau$	$(\mathrm{Re}[V_L], \mathrm{Im}[V_L])$	$(-2.224, -1.228)$	$(0.225, 1.225)$
	$(\mathrm{Re}[V_R], \mathrm{Im}[V_R])$	$(-0.129, -0.906)$	$(0.173, 0.89)$
	$(\mathrm{Re}[S_L], \mathrm{Im}[S_L])$	$(-0.116, -0.788)$	$(0.474, 0.8)$
	$(\mathrm{Re}[S_R], \mathrm{Im}[S_R])$	$(-1.076, -0.809)$	$(0.06, 0.807)$
	$(\mathrm{Re}[T_L], \mathrm{Im}[T_L])$	$(-0.0094, -0.028)$	$(0.0467, 0.028)$

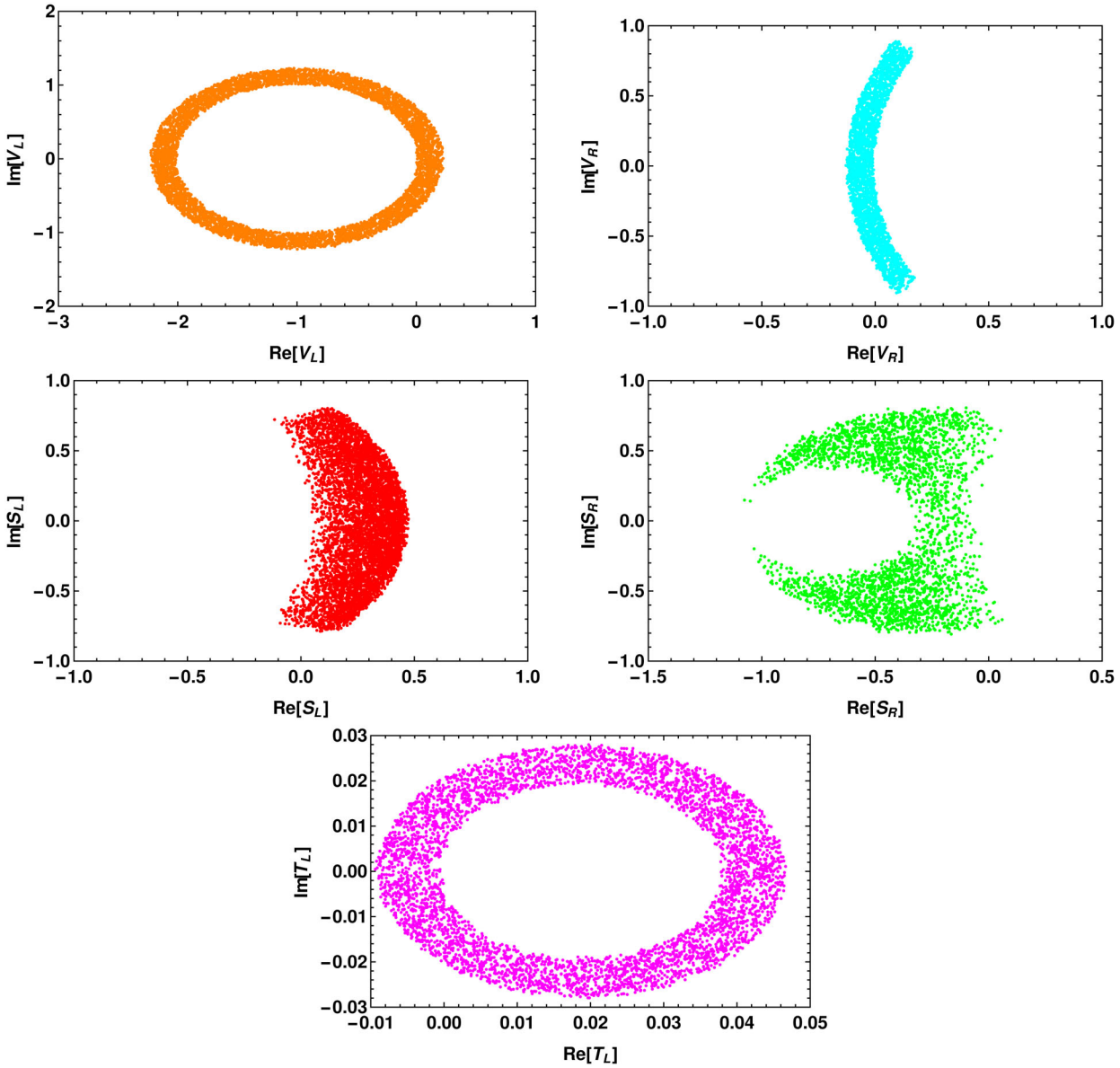

FIG. 2. Constraints on V_L (top left panel), V_R (top right panel), S_L (middle left panel), S_R (middle right panel), and T_L (bottom panel) new coefficients associated with $b \to c\tau\bar{\nu}_\tau$ transitions, obtained from the $\mathrm{Br}(\mathrm{B}_c^+ \to \tau^+\nu_\tau)$, $R_{D^{(*)}}$, and $R_{J/\psi}$ observables. Here the constraint on the T_L coupling is obtained from $R_{D^{(*)}}$ experimental data.

$$f_i(q^2) = \frac{1}{1 - q^2/(m^f_{\rm pole})^2}[a^f_0 + a^f_1 z(q^2)], \quad (i = +, \perp, 0), \tag{28}$$

where $m^f_{\rm pole}$ is the pole mass and

$$z(q^2) = \frac{\sqrt{t_+ - q^2} - \sqrt{t_+ - t_0}}{\sqrt{t_+ - q^2} + \sqrt{t_+ - t_0}}, \tag{29}$$

with $t_\pm = (M_{B_1} \pm M_{B_2})^2$. The values of the parameters $m^f_{\rm pole}$, $a^f_{0,1}$ associated with (axial)vector and (pseudo)scalar form factors ($f_{+,\perp,0}$, $g_{+,\perp,0}$) are taken from [28]. In the lattice QCD approach, the $m^f_{\rm pole}$, $a^f_{0,1}$ parameters linked to tensor form factors ($h_{+,\perp}$, $\tilde{h}_{+,\perp}$) of the $\Lambda_b \to \Lambda_c l\bar{\nu}_l$ process are computed in [32]. However, currently no lattice results are available on the tensor form factors associated with the $\Lambda_b \to p l\bar{\nu}_l$ process. Hence, we relate the tensor form factors of the $\Lambda_b \to p l\bar{\nu}_l$ decay mode with its (axial)vector form factors by using the HQET relations as [33,51,52]

$$f_T = g_T = f_1 = \frac{(M_{B_1} + M_{B_2})^2 f_+ - q^2 f_\perp}{(M_{B_1} + M_{B_2})^2 - q^2},$$
$$f^V_T = g^V_T = f^S_T = g^S_T = 0. \tag{30}$$

The detailed relations between the helicity form factors ($f_{+,\perp,0}$, $g_{+,\perp,0}$, $h_{+,\perp}$, $\tilde{h}_{+,\perp}$) with other various hadronic form factors ($f_{1,2,3}$, $g_{1,2,3}$, f_T, g_T, $f^{V(S)}_T$, $g^{V(S)}_T$) are listed in Appendix B [51]. Using all these input parameters, the predicted branching ratios of the $\Lambda_b \to (\Lambda_c, p)\mu\bar{\nu}_\mu$ processes in the SM are given by

$$\mathrm{Br}(\Lambda_b \to p\mu^-\bar{\nu}_\mu)|^{\rm SM} = (4.31 \pm 0.345) \times 10^{-4},$$
$$\mathrm{Br}(\Lambda_b \to \Lambda_c\mu^-\bar{\nu}_\mu)|^{\rm SM} = (4.994 \pm 0.4) \times 10^{-2}, \tag{31}$$

which are in reasonable agreement with the corresponding experimental data [17]

$$\mathrm{Br}(\Lambda_b \to p\mu^-\bar{\nu}_\mu) = (4.1 \pm 1.0) \times 10^{-4},$$
$$\mathrm{Br}(\Lambda_b \to \Lambda_c l^-\bar{\nu}_l) = (6.2^{+1.4}_{-1.3}) \times 10^{-2}. \tag{32}$$

The values of the forward-backward asymmetries in these channels are found to be

$$\langle A^\mu_{\rm FB}\rangle|^{\rm SM}_{\Lambda_b \to p} = 0.316 \pm 0.025,$$
$$\langle A^\mu_{\rm FB}\rangle|^{\rm SM}_{\Lambda_b \to \Lambda_c} = 0.19 \pm 0.0152. \tag{33}$$

In Eqs. (31) and (33), the theoretical uncertainties are mainly due to the uncertainties associated with the CKM matrix elements and the form factor parameters. After having an idea about all the required input parameters and the allowed parameter space of new couplings, we now proceed to discuss various new physics scenarios and their impact on $\Lambda_b \to (\Lambda_c, p)\tau\bar{\nu}_\tau$ decay modes in a model-independent way.

A. Scenario A: Only V_L coefficient

In this scenario, we assume that the additional new physics contribution to the SM result is coming only from the coupling associated with the left-handed vectorlike quark currents, i.e., $V_L \neq 0$ and V_R, $S_{L,R}$, $T_L = 0$. Since in this case the NP operator has the same Lorentz structure as the SM operator, the SM decay rate gets modified by the factor $|1 + V_L|^2$. Imposing a 3σ constraint on the $\mathrm{Br}(B^+_{u,c} \to \tau^+\nu_\tau)$, $\mathrm{Br}(B^0 \to \pi^+\tau^-\bar{\nu}_\tau)$, R^l_π, $R_{D^{(*)}}$, and $R_{J/\psi}$ observables, the allowed parameter space of V_L couplings associated with $b \to (u, c)\tau\nu_\tau$ is shown in Figs. 1 and 2. Using the minimum and maximum values of the real and imaginary parts of the V_L coefficient from Table II, we present the differential branching ratios of the $\Lambda_b \to p\tau^-\bar{\nu}_\tau$

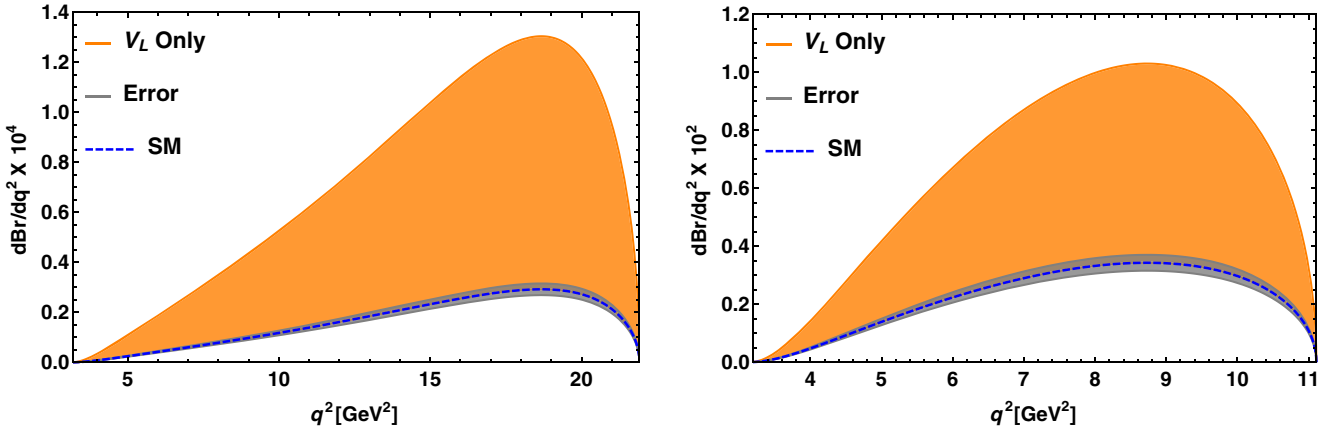

FIG. 3. The q^2 variation of the branching ratio of the $\Lambda_b \to p\tau^-\bar{\nu}_\tau$ (left panel) and $\Lambda_b \to \Lambda^+_c\tau^-\bar{\nu}_\tau$ (right panel) processes in the presence of only the V_L new coefficient. Here the orange bands represent the new physics contribution. Blue dashed lines stand for the SM and the theoretical uncertainties arising due to the input parameters are presented in gray.

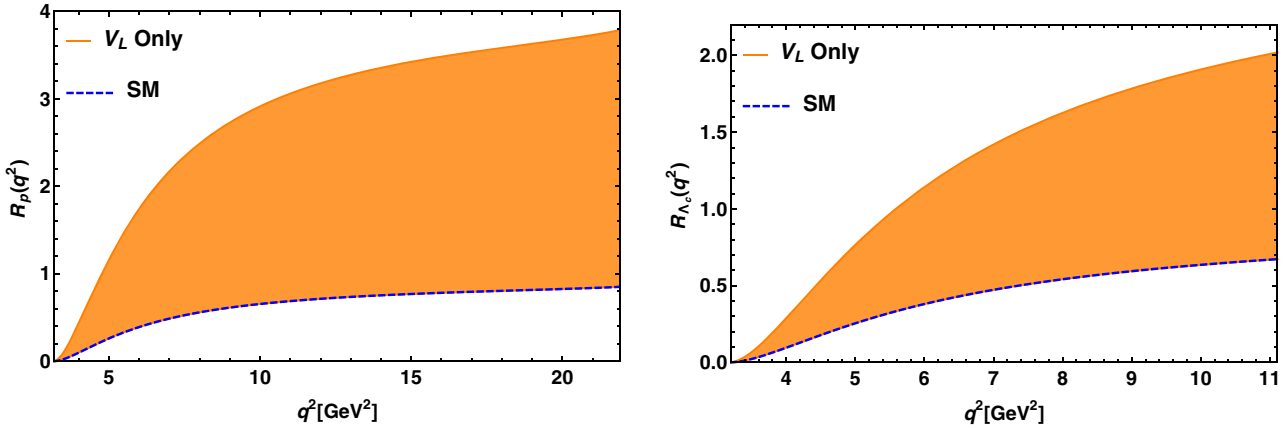

FIG. 4. The variation of the R_p (left panel) and R_{Λ_c} (right panel) LNU parameters with respect to q^2 in the presence of only the V_L new coefficient.

(left panel) and $\Lambda_b \to \Lambda_c \tau^- \bar{\nu}_\tau$ (right panel) processes with respect to q^2 in Fig. 3. In these figures, the blue dashed lines represent the SM contribution, the orange bands are due to the presence of the new V_L coefficient, and the gray bands stand for the theoretical uncertainties associated with the input parameters like form factors, CKM matrix elements, etc. The branching ratios of $\Lambda_b \to (\Lambda_c, p)\tau^- \bar{\nu}_\tau$ deviate significantly from their corresponding SM values due to the NP contribution. In addition to the decay rate, other interesting observables, which can be used to probe new physics, are the zero crossing of the forward-backward asymmetry and the convexity parameters. From Eq. (12), one can notice that the convexity parameter depends only on the $V_{L,R}$ and T_L couplings. The values for the forward-backward asymmetries of the $\Lambda_b \to (\Lambda_c, p)\tau\bar{\nu}_\tau$ processes in the SM are

$$\begin{aligned} \langle A_{\rm FB}^\tau \rangle|^{\rm SM}_{\Lambda_b \to p} &= 0.115 \pm 0.0092, \\ \langle A_{\rm FB}^\tau \rangle|^{\rm SM}_{\Lambda_b \to \Lambda_c} &= -0.09 \pm 0.007, \end{aligned} \tag{34}$$

and the corresponding values for the convexity parameters are

$$\begin{aligned} \langle C_F^\tau \rangle|^{\rm SM}_{\Lambda_b \to p} &= -0.157 \pm 0.013, \\ \langle C_F^\tau \rangle|^{\rm SM}_{\Lambda_b \to \Lambda_c} &= -0.098 \pm 0.008. \end{aligned} \tag{35}$$

We found no deviation from the SM results for the forward-backward asymmetry and convexity parameters due to the presence of the V_L coefficient. In Fig. 4, the left (right) panel depicts the q^2 variation of lepton universality violating parameters $R_p(R_{\Lambda_c})$. We observe that the NP contribution coming from the V_L coupling has a significant impact on the R_p and R_{Λ_c} parameters. The variation of the $R^\tau_{\Lambda_c p}$ parameter with q^2 for this case is presented in the left panel of Fig. 7. The numerical values of the branching ratios and the LNU parameters for both the SM and the V_L-type NP scenario are given in Table III. Besides the branching ratios, forward-backward asymmetry, and LNU parameters of the $\Lambda_b \to (\Lambda_c, p)\tau\bar{\nu}_\tau$ processes, the NP effects can also be observed in the hadron and lepton polarization asymmetries. However, no deviation has been found in the presence of V_L coupling from their corresponding SM results.

B. Scenario B: Only V_R coefficient

Here, we assume that only the new V_R coefficient is present in addition to the SM contribution, in the effective Lagrangian (5). To investigate the effect of NP coming from the V_R coefficient, we first constrain the new coefficient by imposing a 3σ experimental bound on the $b \to (u, c)\tau\bar{\nu}_\tau$ anomalies. Using the values from Table II, we show the plots for the branching ratios of the

TABLE III. The predicted values of the branching ratios and lepton nonuniversality parameters of the $\Lambda_b \to (\Lambda_c, p)\tau\bar{\nu}_\tau$ processes in the SM and in the presence of only the $V_{L,R}$ coefficients.

Observables	SM prediction	Values for V_L coupling	Values for V_R coupling
$\mathrm{Br}(\Lambda_b \to p\tau^-\bar{\nu}_\tau)$	$(2.98 \pm 0.238) \times 10^{-4}$	$(0.298 - 1.34) \times 10^{-3}$	$(2.98 - 8.17) \times 10^{-4}$
R_p	0.692	0.692–3.09	0.692–1.895
$\mathrm{Br}(\Lambda_b \to \Lambda_c^+\tau^-\bar{\nu}_\tau)$	$(1.76 \pm 0.14) \times 10^{-2}$	$(1.76 - 5.29) \times 10^{-2}$	$(1.76 - 3.4) \times 10^{-2}$
R_{Λ_c}	0.353	0.353–1.06	0.353–0.68
$R_{\Lambda_c p}$	$(1.693 \pm 0.19) \times 10^{-2}$	$(1.693 - 2.533) \times 10^{-2}$	$(1.693 - 2.4) \times 10^{-2}$

$\Lambda_b \to p(\Lambda_c)\tau\bar{\nu}_\tau$ process in the top left panel (top right panel) of Fig. 5. In these figures, the cyan bands are due to the additional contribution from the V_R coefficient. We notice a significant deviation in the branching ratios from their corresponding SM results. The predicted values of the branching ratios for the V_R coefficient are presented in Table III. Apart from the branching ratios, we are also interested to see the effect of this new coefficient on various q^2-dependent observables. The q^2 variation of the forward-backward asymmetry and the convexity parameters for the $\Lambda_b \to p\tau^-\bar{\nu}_\tau$ (left) and $\Lambda_b \to \Lambda_c\tau^-\bar{\nu}_\tau$ (right) decay processes are depicted in the middle and bottom panels of Fig. 5, respectively. The deviation of convexity parameters from their SM prediction is not so significant. In the presence of the V_R coefficient, the numerical values of the C_F^τ parameters are

$$\langle C_F^\tau \rangle|^{V_R}_{\Lambda_b\to p} = -0.169 \to -0.147,$$
$$\langle C_F^\tau \rangle|^{V_R}_{\Lambda_b\to \Lambda_c} = -0.105 \to -0.094. \quad (36)$$

The effect of the V_R coefficient is found to be rather significant on the forward-backward asymmetry observables of both $\Lambda_b \to p(\Lambda_c)\tau^-\bar{\nu}_\tau$ decay modes, and the corresponding numerical values are

$$\langle A_{\rm FB}^\tau \rangle|^{V_R}_{\Lambda_b\to p} = -0.248 \to 0.115,$$
$$\langle A_{\rm FB}^\tau \rangle|^{V_R}_{\Lambda_b\to \Lambda_c} = -0.23 \to -0.09. \quad (37)$$

The left and right panels of Fig. 6 depict the variation of R_p and R_{Λ_c} parameters with respect to q^2. Though there are no experimental limits on these parameters, significant

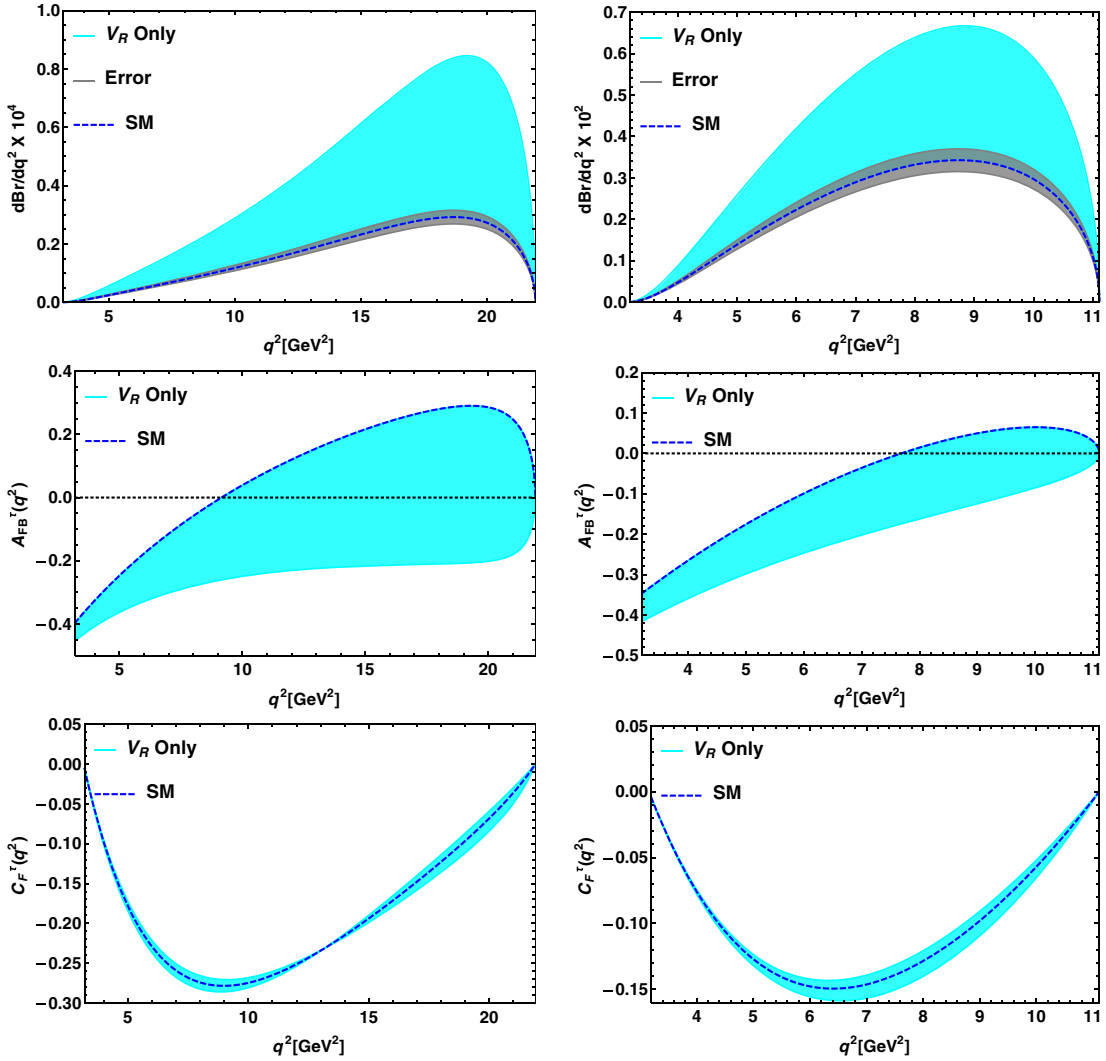

FIG. 5. The top panel represents the q^2 variation of the branching ratio of $\Lambda_b \to p\tau^-\bar{\nu}_\tau$ (left panel) and $\Lambda_b \to \Lambda_c^+\tau^-\bar{\nu}_\tau$ (right panel) for only the V_R new coefficient. The corresponding plots of forward-backward asymmetry and the convexity parameters are shown in the middle and bottom panels, respectively. Here cyan bands are due to the additional new physics contribution coming from only the V_R coefficient.

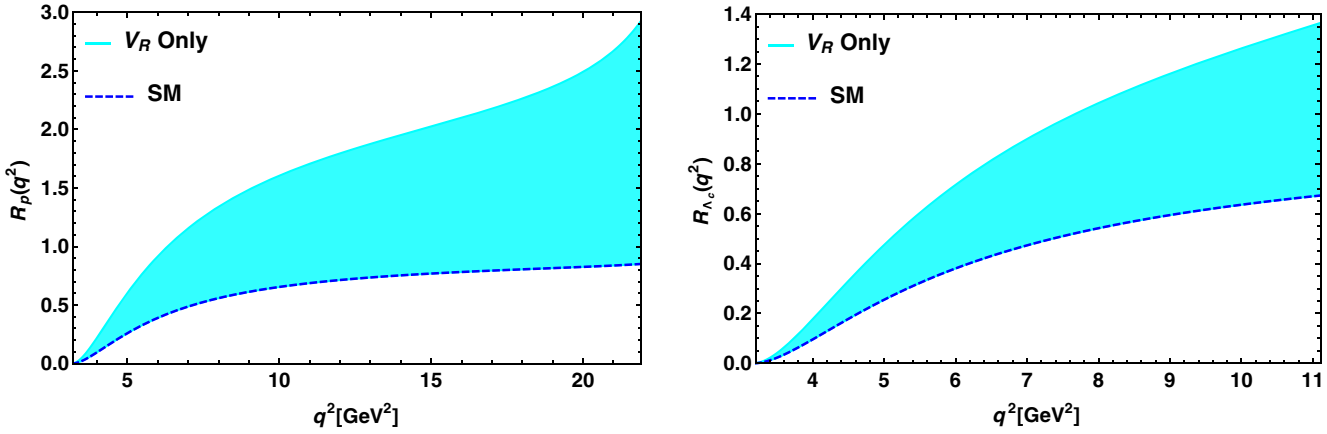

FIG. 6. The variation of the R_p (left panel) and R_{Λ_c} (right panel) LNU parameters with respect to q^2 in the presence of only the V_R new coefficient.

deviation from their SM values is noticed in the scenario with only the V_R coupling. The right panel of Fig. 7 represents the q^2 variation of the $R^{\tau}_{\Lambda_c p}$ parameter. The corresponding numerical values are listed in Table III.

Though the presence of the V_L coefficient has no effect on the lepton and hadron polarization asymmetries of $b \to (u, c)\tau\bar{\nu}_\tau$ decay modes, the V_R coefficient has a significant impact on these parameters. In the top panel of Fig. 8, the distribution of the longitudinal polarization components of the daughter baryon p (left panel) and Λ_c (right panel) are shown both in the SM and in the presence of only the V_R coefficient, and the corresponding plots for the charged τ lepton are presented in the bottom panel. The integrated values of the hadron longitudinal polarization asymmetry parameters in the full physical phase space are

$$\langle P_L^p \rangle|^{\rm SM}_{\Lambda_b \to p} = -0.897, \qquad \langle P_L^{\Lambda_c} \rangle|^{\rm SM}_{\Lambda_b \to \Lambda_c} = -0.797, \tag{38}$$

$$\langle P_L^p \rangle|^{V_R\ {\rm Only}}_{\Lambda_b \to p} = -0.897 \to 0.276,$$
$$\langle P_L^{\Lambda_c} \rangle|^{V_R\ {\rm Only}}_{\Lambda_b \to \Lambda_c} = -0.797 \to -0.068, \tag{39}$$

and the corresponding numerical values for the charged lepton τ are

$$\langle P_L^\tau \rangle|^{\rm SM}_{\Lambda_b \to p} = -0.514, \qquad \langle P_L^\tau \rangle|^{\rm SM}_{\Lambda_b \to \Lambda_c} = -0.207, \tag{40}$$

$$\langle P_L^\tau \rangle|^{V_R}_{\Lambda_b \to p} = -0.577 \to -0.433,$$
$$\langle P_L^\tau \rangle|^{V_R}_{\Lambda_b \to \Lambda_c} = -0.25 \to -0.146. \tag{41}$$

C. Scenario C: Only S_L coefficient

Here, we explore the impact of only the S_L coefficient on the angular observables of heavy-heavy and heavy-light semileptonic decays of Λ_b baryons. In Sec. III, we discussed the constraints on the S_L coupling. In the top

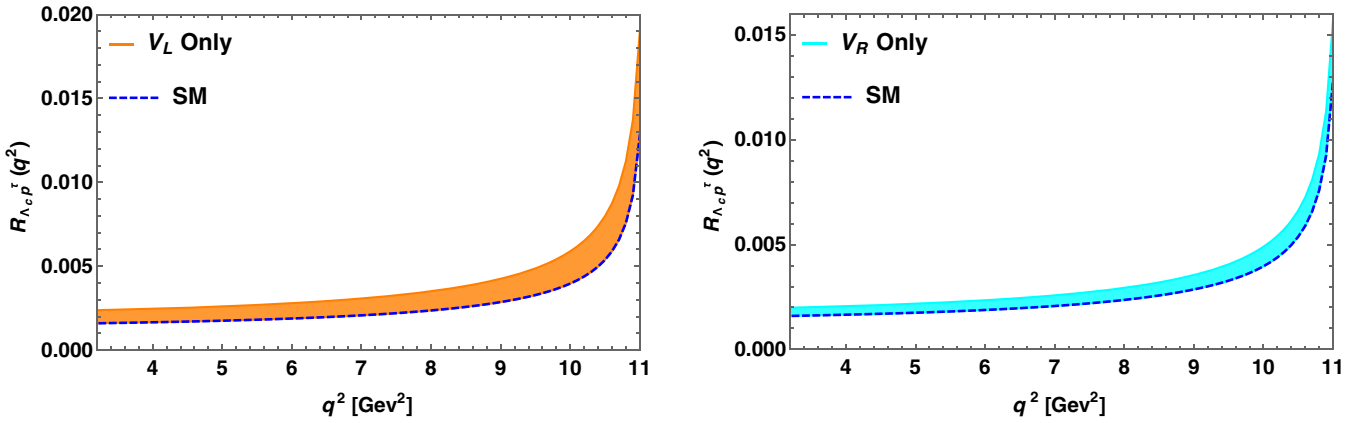

FIG. 7. The variation of the $R^{\tau}_{\Lambda_c p}$ parameter with respect to q^2 in the presence of only the V_L (left panel) and V_R (right panel) new coefficients.

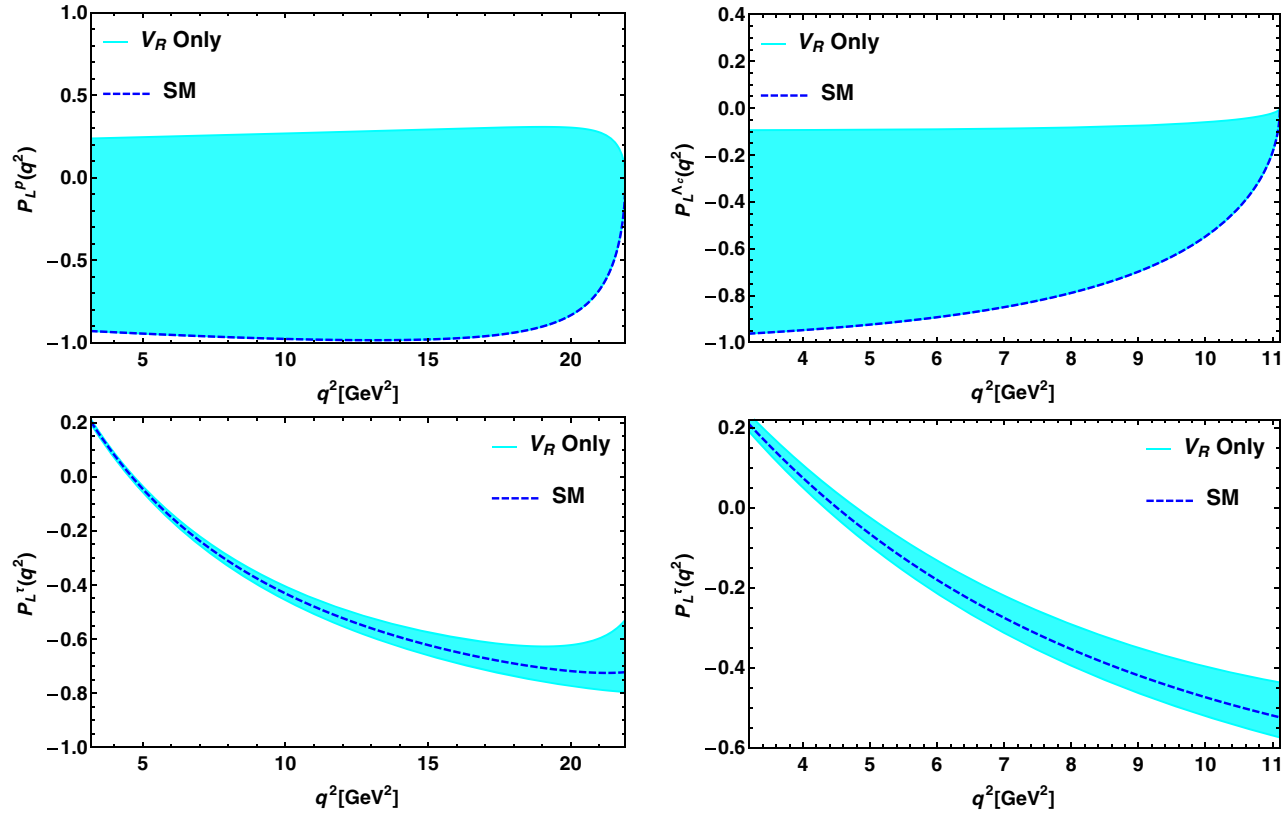

FIG. 8. The plots in the left panel represent the longitudinal polarizations of the daughter light baryon p (left top panel) and the charged τ lepton (left bottom) with respect to q^2 for only the V_R coefficient. The corresponding plots for the $\Lambda_b \to \Lambda_c \tau^- \bar{\nu}_\tau$ mode are shown in the right panel.

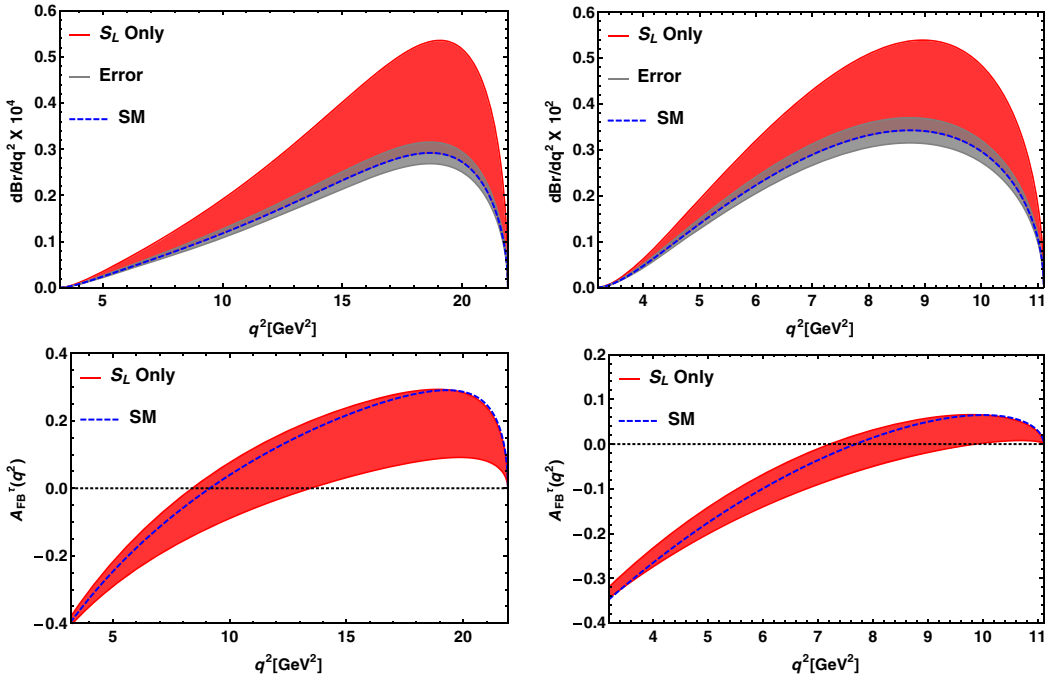

FIG. 9. The top panel represents the q^2 variation of the branching ratios of the $\Lambda_b \to p\tau^-\bar{\nu}_\tau$ (left panel) and $\Lambda_b \to \Lambda_c^+ \tau^- \bar{\nu}_\tau$ (right panel) decay modes in the presence of only the S_L new coefficient. The corresponding plots for forward-backward asymmetries are shown in the bottom panel. Here red bands are due to the additional new physics contribution coming from only the S_L coefficient.

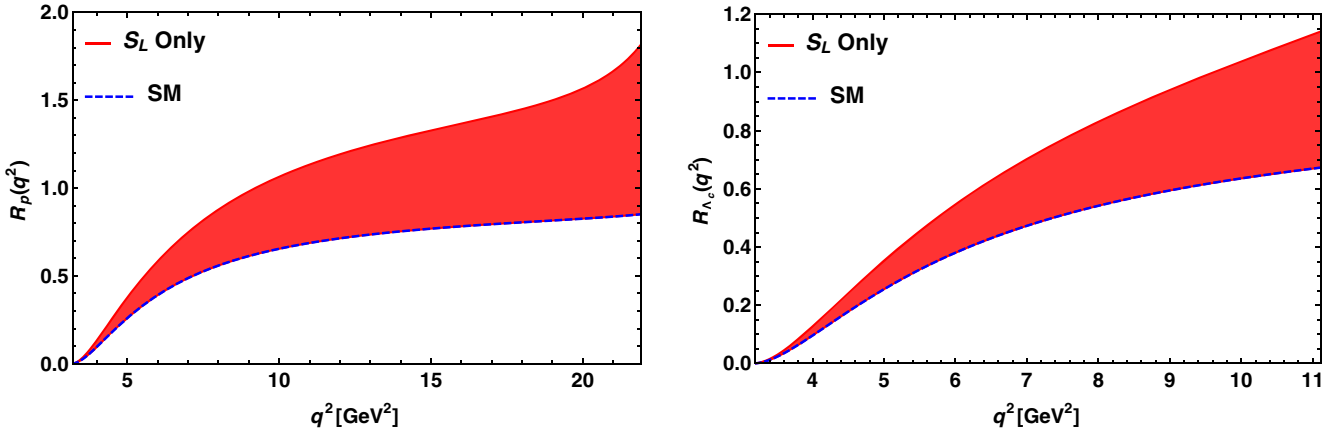

FIG. 10. The variation of R_p (left panel) and R_{Λ_c} (right panel) with respect to q^2 in the presence of only the S_L coefficient.

panel of Fig. 9, we present the plots for the differential branching ratios of the $\Lambda_b \to p\tau\bar{\nu}_\tau$ (left) and $\Lambda_b \to \Lambda_c\tau\bar{\nu}_\tau$ (right) decay processes with respect to q^2 in the presence of the S_L coefficient. The corresponding plots for the forward-backward asymmetry are shown in the bottom panel. In these figures, the red bands stand for the NP contribution from the S_L coefficient. The additional contributions provide a deviation in the branching ratios and forward-backward asymmetries from their SM values. The q^2 variation of the R_p (left panel) and R_{Λ_c} (right panel) LNU parameters in the presence of S_L coupling is given in Fig. 10. In the presence of only the S_L coupling, the longitudinal polarization components of the p (top left panel) and Λ_c (top right panel) daughter baryons with respect to q^2 are presented in

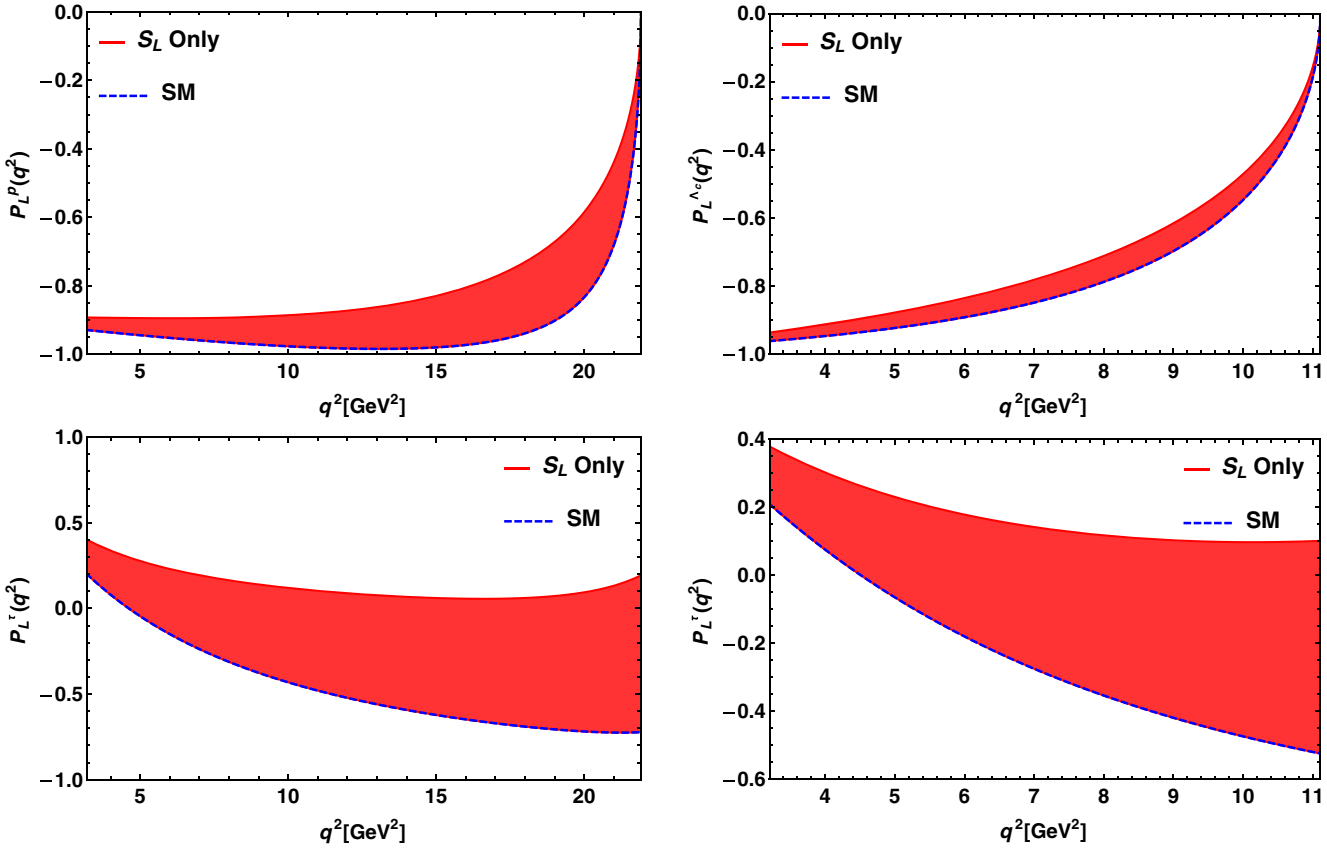

FIG. 11. The plots in the left panel represent the longitudinal polarizations of the daughter light baryon p (left top panel) and the charged τ lepton (left bottom) with respect to q^2 for only the S_L coefficient. The corresponding plots for the $\Lambda_b \to \Lambda_c\tau^-\bar{\nu}_\tau$ mode are shown in the right panel.

TABLE IV. The predicted values of branching ratios, forward-backward asymmetries, longitudinal hadron and lepton polarization asymmetries, and lepton nonuniversality parameters of the $\Lambda_b \to (\Lambda_c, p)\tau\bar{\nu}_\tau$ processes in the SM and in the presence of only the $S_{L,R}$ and T_L new coefficients.

Observables	Values for S_L coupling	Values for S_R coupling	Values for T_L coupling
$\mathrm{Br}(\Lambda_b \to p\tau^-\bar{\nu}_\tau)$	$(2.98 - 5.25) \times 10^{-4}$	$(2.98 - 3.48) \times 10^{-4}$	$(0.298 - 6.68) \times 10^{-3}$
A_{FB}^{τ}	$-0.019 \to 0.139$	$0.086 \to 0.177$	$-0.172 \to -0.125$
P_L^p	$-0.896 \to -0.73$	$-0.896 \to -0.6$	$-0.896 \to 0.337$
P_L^{τ}	$-0.515 \to 0.123$	$-0.515 \to -0.31$	$-0.515 \to 0.037$
R_p	0.692–1.266	0.692–0.81	0.692–8.8
$\mathrm{Br}(\Lambda_b \to \Lambda_c^+\tau^-\bar{\nu}_\tau)$	$(1.76 - 2.7) \times 10^{-2}$	$(1.76 - 2.2) \times 10^{-2}$	$(1.553 - 1.82) \times 10^{-2}$
A_{FB}^{τ}	$-0.121 \to -0.06$	$-0.786 \to -0.005$	$-0.034 \to -0.09$
$P_L^{\Lambda_c}$	$-0.796 \to -0.725$	$-0.796 \to -0.4$	$-0.79 \to -0.812$
P_L^{τ}	$-0.207 \to 0.178$	$-0.207 \to -0.0021$	-0.207
R_{Λ_c}	0.353–0.539	0.353–0.44	$0.31 \to 0.364$
$R_{\Lambda_c p}$	$(1.693 - 1.95) \times 10^{-2}$	$(1.582 - 1.693) \times 10^{-2}$	0.0192–0.367

the top panel of Fig. 11 and the bottom panel depicts the longitudinal lepton polarization asymmetry parameters for the $\Lambda_b \to p(\Lambda_c)\tau\bar{\nu}_\tau$ processes. The lepton polarization asymmetry parameters provide a profound deviation from the SM in comparison to their longitudinal hadron polarization parameters. The top left panel of Fig. 18 shows the variation of the $R_{\Lambda_c p}^{\tau}$ parameter with q^2. In Table IV, we report the numerical values of all these parameters.

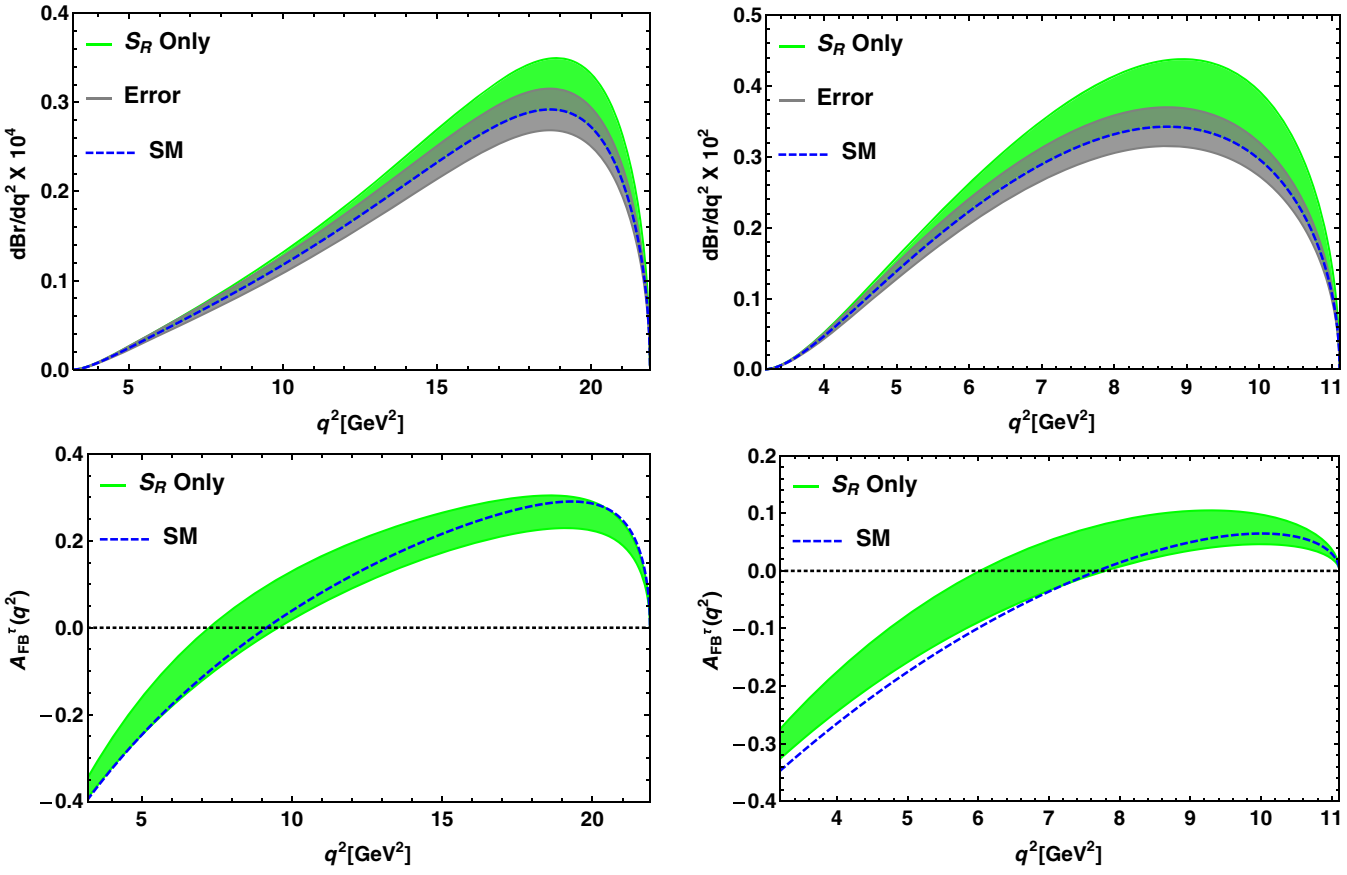

FIG. 12. The top panel represents the q^2 variation of the branching ratios of the $\Lambda_b \to p\tau^-\bar{\nu}_\tau$ (left panel) and $\Lambda_b \to \Lambda_c^+\tau^-\bar{\nu}_\tau$ (right panel) decay processes in the presence of only the S_R coefficient. The corresponding plots for the forward-backward asymmetries are shown in the bottom panel. Here green bands stand for the additional new physics contribution coming from only the S_R coefficient.

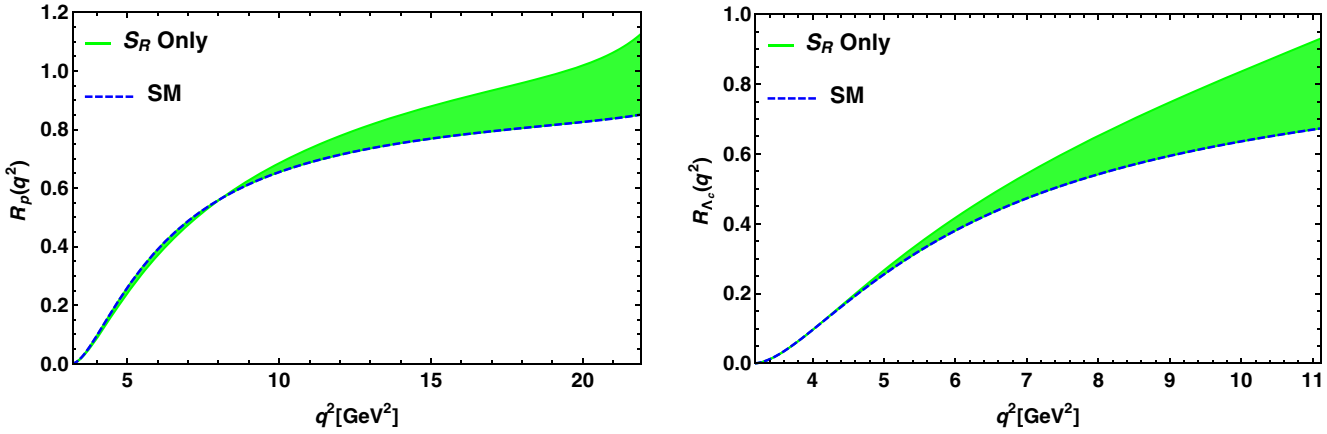

FIG. 13. The variation of R_p (left panel) and R_{Λ_c} (right panel) with respect to q^2 in the presence of only the S_R coefficient.

D. Scenario D: Only S_R coefficient

In this subsection, we perform an analysis for the semileptonic decay modes of Λ_b baryons with the additional S_R coupling. Using the allowed ranges of the real and imaginary part of S_R coupling from Table II, the branching ratios of the $\Lambda_b \to p\tau\bar{\nu}_\tau$ (left) and $\Lambda_b \to \Lambda_c\tau\bar{\nu}_\tau$ (right) decay processes with respect to q^2 are presented in Fig. 12. The bottom panel of this figure represents the q^2 variation of the forward-backward asymmetry for $\Lambda_b \to p\tau\bar{\nu}_\tau$ (left) and $\Lambda_b \to \Lambda_c\tau\bar{\nu}_\tau$ (right). In these figures, the green bands are due to the additional new contribution of the S_R coefficient to the SM. We observe a profound deviation in the branching ratios and forward-backward asymmetries of these decay modes from their SM values. The left (right) panel of Fig. 13 shows the effect of S_R coupling on the q^2 variation of the R_p (R_{Λ_c}) parameter. The longitudinal polarization components of the

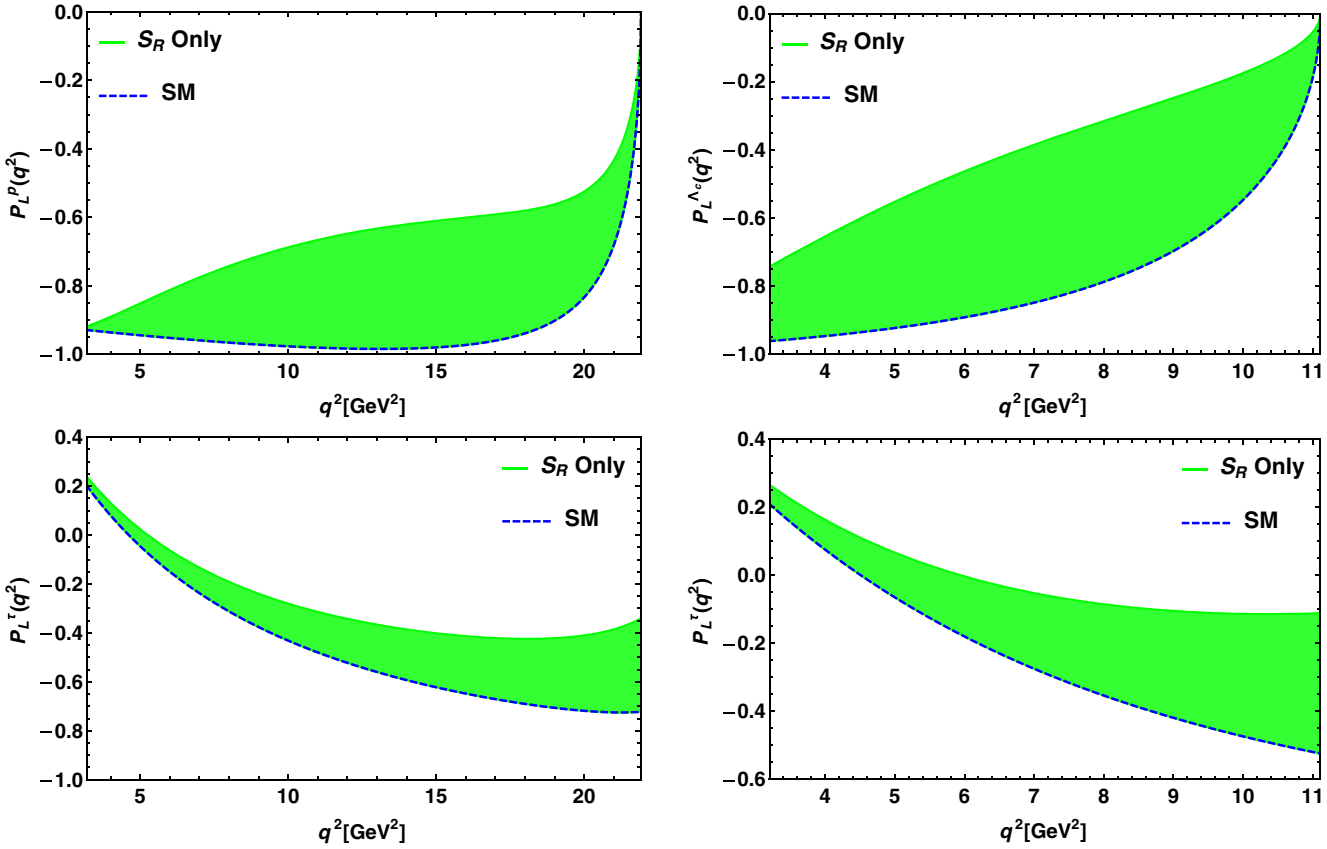

FIG. 14. The plots in the left panel represent the longitudinal polarizations of the daughter light baryon p (left top panel) and the charged τ lepton (left bottom) with respect to q^2 for only the S_R coefficient. The corresponding plots for the $\Lambda_b \to \Lambda_c\tau^-\bar{\nu}_\tau$ mode are shown in the right panel.

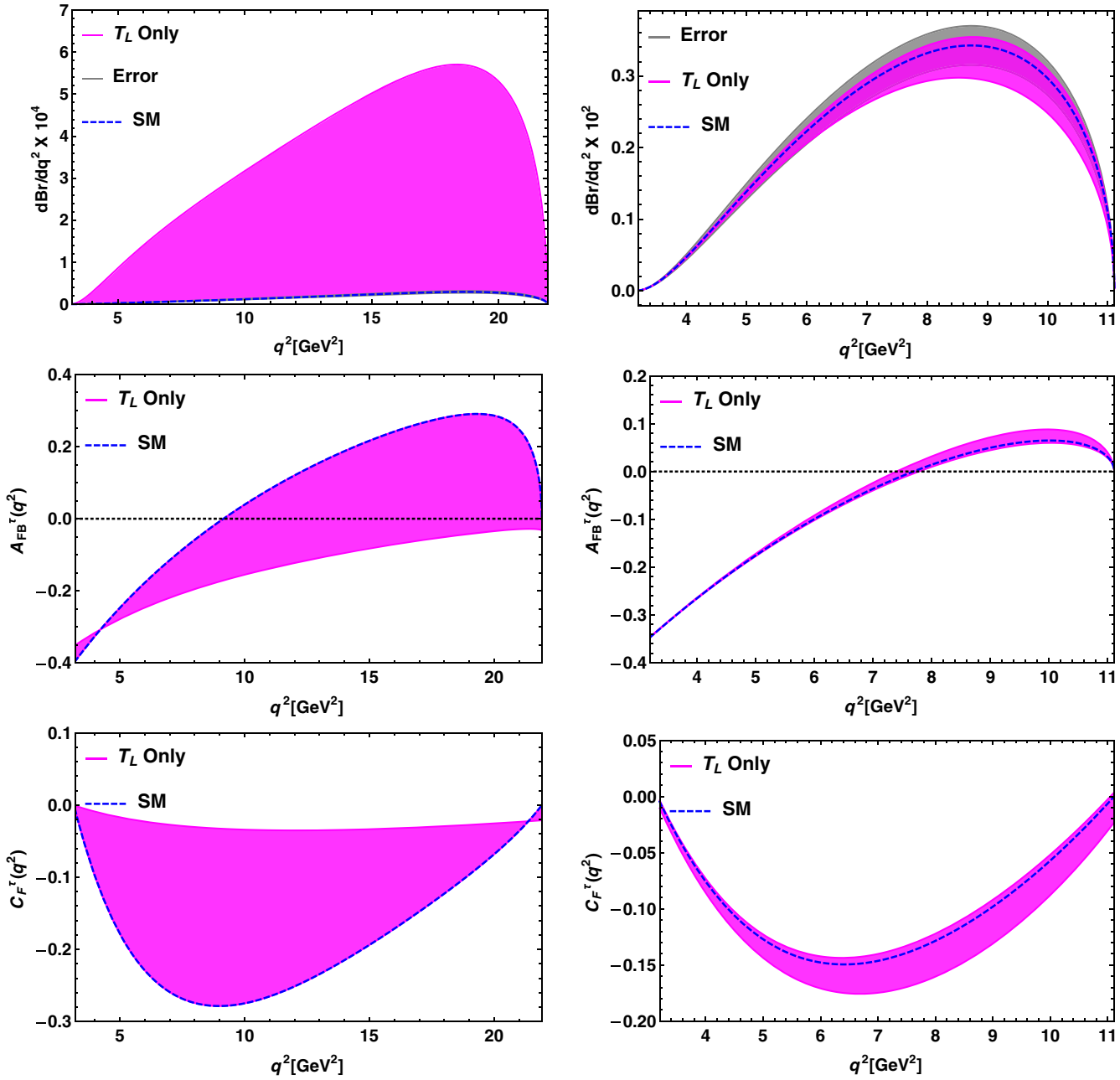

FIG. 15. The top panel represents the q^2 variation of the branching ratio of $\Lambda_b \to p\tau^-\bar{\nu}_\tau$ (left panel) and $\Lambda_b \to \Lambda_c^+\tau^-\bar{\nu}_\tau$ (right panel) for only the T_L new coefficient. The corresponding plots of forward-backward asymmetry and the convexity parameters are shown in the middle and bottom panels, respectively. Here magenta bands are due to the additional new physics contribution coming from only the T_L coefficient.

p (top left panel) and Λ_c (top right panel) daughter baryons with respect to q^2 in the presence of the contribution from only the S_R coefficient are presented in the top panels of Fig. 14, and the bottom panels depict the longitudinal lepton polarization asymmetry parameters for the $\Lambda_b \to p(\Lambda_c)\tau\bar{\nu}_\tau$ processes. We notice significant deviation of the hadron and lepton polarization asymmetries from their corresponding SM values due to the additional contribution from the S_R coupling. The plot for the $R^\tau_{\Lambda_c p}$ parameter with q^2 in the presence of only the S_R coefficient is presented in the right panel of Fig. 18. The numerical values of all these parameters are presented in Table IV. Since the convexity parameters are independent of scalar-type couplings, the $S_{L,R}$ coefficients play no role for this parameter.

E. Scenario E: Only T_L coefficient

The sensitivity of tensor coupling on various physical observables associated with semileptonic baryonic $b \to (c, u)\tau\bar{\nu}_\tau$ decay processes will be investigated in this

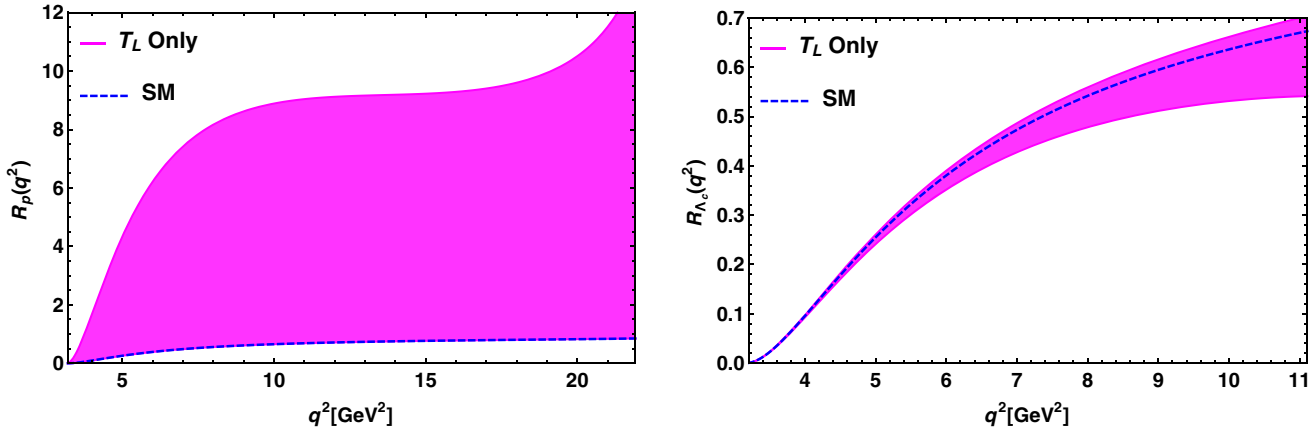

FIG. 16. The variation of R_p (left panel) and R_{Λ_c} (right panel) with respect to q^2 in the presence of only the T_L coefficient.

subsection. The allowed region of real and imaginary parts of the tensor coupling is presented in Sec. III. Using all the input parameters and the constrained new tensor coefficient, we show the q^2 variation of the branching ratio (left top panel), forward-backward asymmetry (left middle panel), and convexity parameter (left bottom panel) of the $\Lambda_b \to p\tau\bar{\nu}_\tau$ decay mode in the left panel of Fig. 15. The right panel of this figure represents the corresponding plots for the $\Lambda_b \to \Lambda_c\tau\bar{\nu}_\tau$ process. Here the magenta bands represent the additional contribution coming from the new T_L coefficient. For the $\Lambda_b \to p\tau\bar{\nu}_\tau$ process, as the bound on T_L is weak, the branching ratio, forward-backward asymmetry, and convexity parameter deviate significantly from their SM predications compared to the observables for the $\Lambda_b \to \Lambda_c\tau\bar{\nu}_\tau$ process. For the $\Lambda_b \to \Lambda_c\tau\bar{\nu}_\tau$ process, the deviations are quite minimal as the

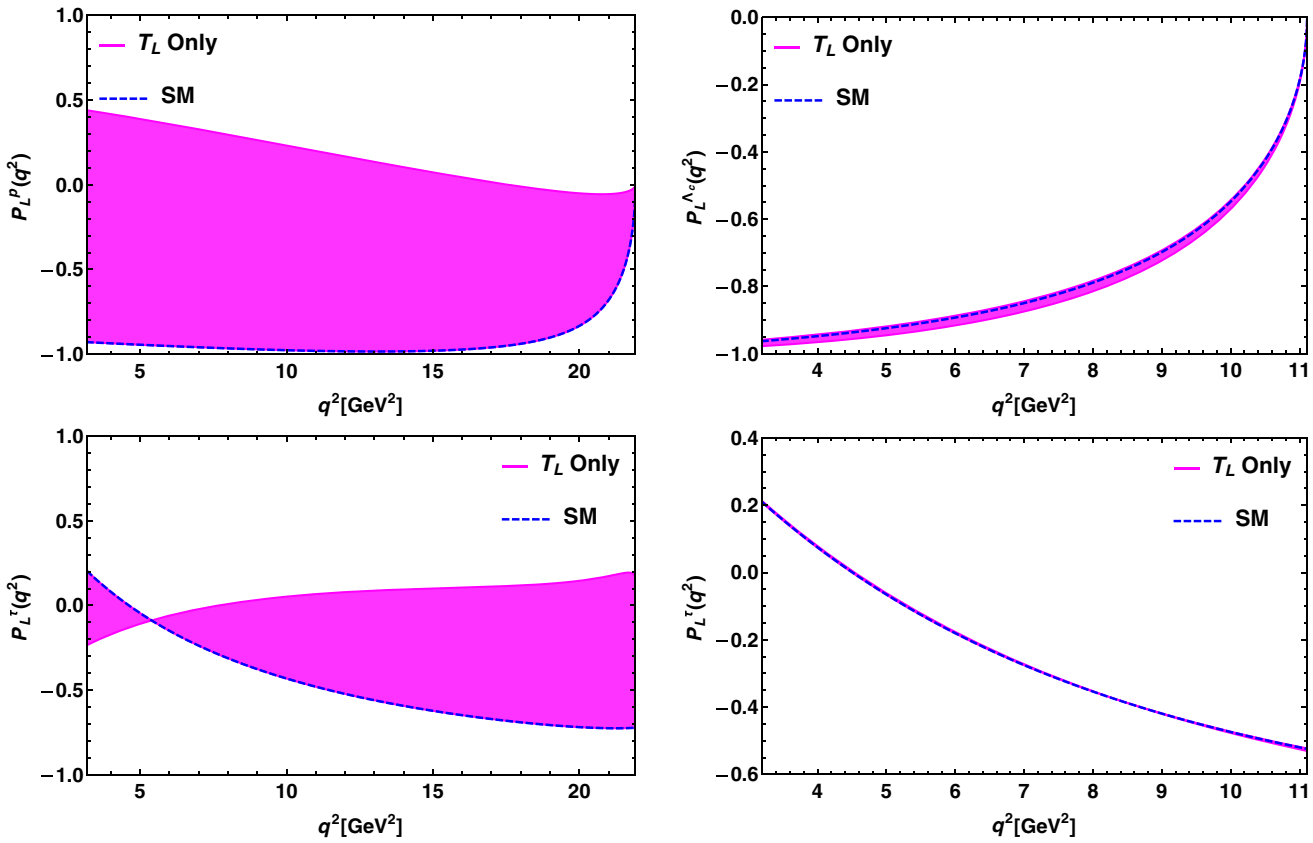

FIG. 17. The plots in the left panel represent the longitudinal polarizations of the daughter light baryon p (left top panel) and the charged τ lepton (left bottom) with respect to q^2 for only the T_L coefficient. The corresponding plots for the $\Lambda_b \to \Lambda_c\tau^-\bar{\nu}_\tau$ mode are shown in the right panel.

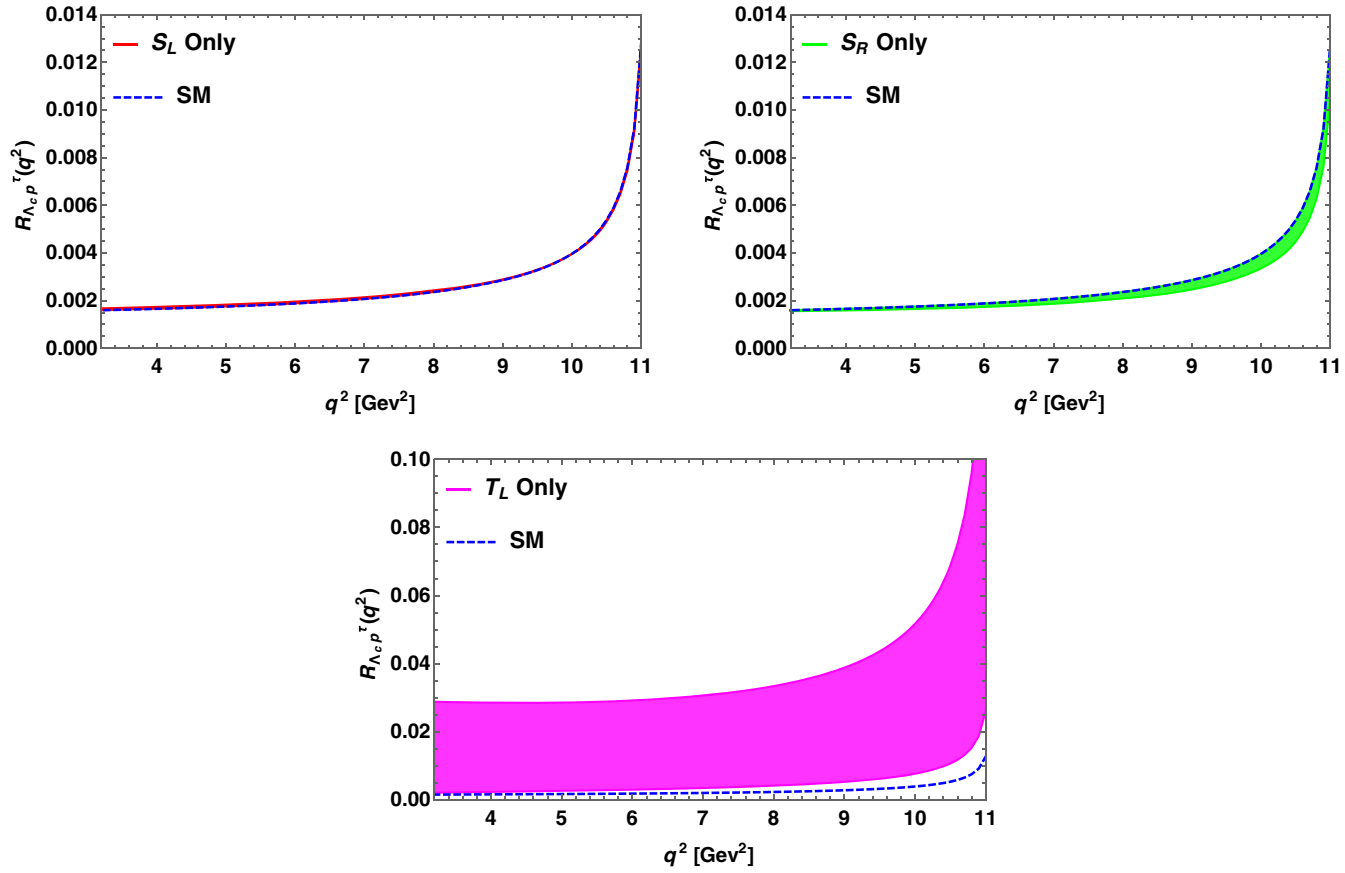

FIG. 18. The variation of the $R^{\tau}_{\Lambda_c p}$ parameter with respect to q^2 in the presence of only the S_L (top left panel), S_R (top right panel), and T_L (bottom panel) coefficients.

coefficient T_L is severely constrained. In the presence of the T_L coefficient, the numerical values of the convexity parameters are

$$\langle C_F^{\tau}\rangle|^{T_L}_{\Lambda_b\to p} = -0.017 \to -0.027,$$
$$\langle C_F^{\tau}\rangle|^{T_L}_{\Lambda_b\to \Lambda_c} = -0.121 \to -0.098. \tag{42}$$

The plots for the lepton nonuniversality parameter R_p (left panel) and R_{Λ_c} (right panel) are shown in Fig. 16. The top panel of Fig. 17 represents the hadron polarization asymmetry parameters of the $\Lambda_b \to p\tau\bar{\nu}_\tau$ (left panel) and $\Lambda_b \to \Lambda_c\tau\bar{\nu}_\tau$ (right panel) process and the corresponding plots for the lepton polarization asymmetries are given in the bottom panel of this figure. We observe that the LNU parameter, longitudinal hadron, and lepton polarization asymmetries of the $\Lambda_b \to p\tau\bar{\nu}_\tau$ process have a large deviation from their SM values due to the presence of tensor coupling, whereas negligible deviations (R_{Λ_c} has some deviation from its SM result) are noticed for the observables of the $\Lambda_b \to \Lambda_c\tau\bar{\nu}_\tau$ decay mode. The q^2 variation of the $R^{\tau}_{\Lambda_c p}$ parameter is depicted in the bottom panel of Fig. 18. Table IV shows the integrated values of all these angular observables.

V. CONCLUSION

In this work, we have performed a model-independent analysis of baryonic $\Lambda_b \to (\Lambda_c, p)l\bar{\nu}_l$ decay processes by considering the generalized effective Lagrangian in the presence of new physics. We considered the new couplings to be complex in our analysis. In order to constrain the new couplings, we have assumed that only one coefficient is present at a time and we have constrained the new coefficients by comparing the theoretical predictions of the $\mathrm{Br}(B^+_{u,c} \to \tau^+\nu_\tau)$, $\mathrm{Br}(B \to \pi\tau\bar{\nu}_\tau)$, R^l_π, $R_{D^{(*)}}$, and $R_{J/\psi}$ observables with their measured experimental data. Using the allowed parameter space, we estimated the branching ratios, forward-backward asymmetries, and convexity parameters of the $\Lambda_b \to (\Lambda_c, p)l\bar{\nu}_\tau$ decay processes. We also investigated the longitudinal polarization components of the daughter baryon (p, Λ_c) and the final state charged lepton, τ. The convexity parameters only depend on the (axial)vector- and tensor-type couplings and are independent of the $S_{L,R}$, T_L coefficients. Inspired by the observation of lepton nonuniversality parameters in various B meson decays, we have also scrutinized the lepton universality violating parameters (R_p, R_{Λ_c}, $R^{\tau}_{\Lambda_c p}$) in the baryonic decay modes. We found significant deviation in the branching

ratios and the R_p, R_{Λ_c}, and $R_{\Lambda_c p}$ parameters from their corresponding Standard Model values, in the presence of additional new vectorlike coupling (V_L coefficient). However, such coupling does not affect the convexity parameter, forward-backward asymmetries, or lepton and hadron polarization asymmetries. We further noticed a profound deviation in the branching ratios and all other angular observables of the semileptonic baryonic $b \to (u, c)\tau\bar{\nu}_l$ decay processes due to the additional contribution of V_R coupling to the SM. The branching ratios, forward-backward asymmetries, longitudinal hadron and lepton polarization asymmetry parameters, and the LNU observables deviate significantly from their corresponding Standard Model results in the presence of $S_{L,R}$ coefficients. These coefficients do not have a significant effect on the $R_{\Lambda_c p}$ parameter. We have also computed the branching ratio, forward-backward asymmetry, convexity parameter, hadron and lepton polarization asymmetries, and LNU parameter of the $\Lambda_b \to p(\Lambda_c)\tau\bar{\nu}_\tau$ decay process by using the additional contribution from new tensor (T_L) coupling. All of the angular observables of the $\Lambda_b \to p\tau\bar{\nu}_\tau$ process receive significant deviations from their SM values, compared to the corresponding parameters of the $\Lambda_b \to \Lambda_c\tau\bar{\nu}_\tau$ decay mode. To conclude, we have explored the effect of individual complex $V_{L,R}$, $S_{L,R}$, and T_L couplings on the angular observables of baryonic decays of Λ_b baryons. We found a profound deviation from the Standard Model results due to the presence of these new couplings. We noticed that the V_R and S_L couplings significantly affect all the observables and the tensor coupling plays a vital role in the case of the $\Lambda_b \to p\tau\bar{\nu}_\tau$ decay mode. Though there is no experimental measurement on these baryonic $b \to (u, c)\tau\bar{\nu}_\tau$ decay processes, the study of these modes is found to be very crucial in order to shed light on the nature of new physics.

ACKNOWLEDGMENTS

R. M. would like to thank the Science and Engineering Research Board (SERB), Government of India, for financial support through Grant No. SB/S2/HEP-017/2013. A. R. acknowledges the University Grants Commission for financial support.

APPENDIX A: HELICITY-DEPENDENT DIFFERENTIAL DECAY RATES

The expressions for the helicity-dependent differential decay rates required to analyze the longitudinal hadron and lepton polarization asymmetries are given by [33]

$$\begin{aligned}
\frac{d\Gamma^{\lambda_2=1/2}}{dq^2} &= \frac{m_l^2}{q^2}\left[\frac{4}{3}(H^2_{\frac{1}{2},+} + H^2_{\frac{1}{2},0} + 3H^2_{\frac{1}{2},t}) + \frac{2}{3}(H^{T^2}_{\frac{1}{2},+,-} + H^{T^2}_{\frac{1}{2},0,t} + H^{T^2}_{\frac{1}{2},+,0} + H^{T^2}_{\frac{1}{2},+,t} + 2H^T_{\frac{1}{2},+,-}H^T_{\frac{1}{2},0,t} + 2H^T_{\frac{1}{2},+,0}H^T_{\frac{1}{2},+,t})\right] \\
&+ \frac{8}{3}(H^2_{\frac{1}{2},0} + H^2_{\frac{1}{2},+}) + 4H^{SP^2}_{\frac{1}{2},0} + \frac{1}{3}(H^{T^2}_{\frac{1}{2},+,-} + H^{T^2}_{\frac{1}{2},0,t} + H^{T^2}_{\frac{1}{2},+,0} + H^{T^2}_{\frac{1}{2},+,t} + 2H^T_{\frac{1}{2},+,-}H^T_{\frac{1}{2},0,t} + 2H^T_{\frac{1}{2},+,0}H^T_{\frac{1}{2},+,t}) \\
&+ \frac{4m_l}{\sqrt{q^2}}[(H_{\frac{1}{2},0}H^T_{\frac{1}{2},+,-} + H_{\frac{1}{2},0}H^T_{\frac{1}{2},0,t} + H_{\frac{1}{2},+}H^T_{\frac{1}{2},+,0} + H_{\frac{1}{2},+}H^T_{\frac{1}{2},+,t}) + 2(H_{\frac{1}{2},t}H^{SP}_{\frac{1}{2},0})], \\
\frac{d\Gamma^{\lambda_2=-1/2}}{dq^2} &= \frac{m_l^2}{q^2}\left[\frac{4}{3}(H^2_{-\frac{1}{2},-} + H^2_{-\frac{1}{2},0} + 3H^2_{-\frac{1}{2},t}) + \frac{2}{3}(H^{T^2}_{-\frac{1}{2},+,-} + H^{T^2}_{-\frac{1}{2},0,t} + H^{T^2}_{-\frac{1}{2},0,-} + H^{T^2}_{-\frac{1}{2},-,t}\right. \\
&\left. + 2H^T_{-\frac{1}{2},+,-}H^T_{-\frac{1}{2},0,t} + 2H^T_{-\frac{1}{2},0,-}H^T_{-\frac{1}{2},-,t})\right] + \frac{8}{3}(H^2_{-\frac{1}{2},-} + H^2_{-\frac{1}{2},0}) + 4H^{SP^2}_{-\frac{1}{2},0} \\
&+ \frac{1}{3}(H^{T^2}_{-\frac{1}{2},+,-} + H^{T^2}_{-\frac{1}{2},0,t} + H^{T^2}_{-\frac{1}{2},0,-} + H^{T^2}_{-\frac{1}{2},-,t} + 2H^T_{-\frac{1}{2},+,-}H^T_{-\frac{1}{2},0,t} + 2H^T_{-\frac{1}{2},0,-}H^T_{-\frac{1}{2},-,t}) \\
&+ \frac{4m_l}{\sqrt{q^2}}[(H_{-\frac{1}{2},0}H^T_{-\frac{1}{2},+,-} + H_{-\frac{1}{2},0}H^T_{-\frac{1}{2},0,t} + H_{-\frac{1}{2},-}H^T_{-\frac{1}{2},0,-} + H_{-\frac{1}{2},-}H^T_{-\frac{1}{2},-,t}) + 2(H_{-\frac{1}{2},t}H^{SP}_{-\frac{1}{2},0})], \\
\frac{d\Gamma^{\lambda_\tau=1/2}}{dq^2} &= \frac{m_l^2}{q^2}\left[\frac{4}{3}(H^2_{\frac{1}{2},+} + H^2_{\frac{1}{2},0} + H^2_{-\frac{1}{2},-} + H^2_{-\frac{1}{2},0}) + 4(H^2_{\frac{1}{2},t} + H^2_{-\frac{1}{2},t})\right] + 4(H^{SP^2}_{\frac{1}{2},0} + H^{SP^2}_{-\frac{1}{2},0}) \\
&+ \frac{1}{3}[H^{T^2}_{\frac{1}{2},+,-} + H^{T^2}_{\frac{1}{2},0,t} + H^{T^2}_{\frac{1}{2},+,0} + H^{T^2}_{\frac{1}{2},+,t} + H^{T^2}_{-\frac{1}{2},+,-} + H^{T^2}_{-\frac{1}{2},0,t} + H^{T^2}_{-\frac{1}{2},0,-} + H^{T^2}_{-\frac{1}{2},-,t} \\
&+ 2(H^T_{\frac{1}{2},+,-}H^T_{\frac{1}{2},0,t} + H^T_{\frac{1}{2},+,0}H^T_{\frac{1}{2},+,t} + H^T_{-\frac{1}{2},+,-}H^T_{-\frac{1}{2},0,t} + H^T_{-\frac{1}{2},0,-}H^T_{-\frac{1}{2},-,t})] \\
&+ \frac{4m_l}{3\sqrt{q^2}}[6(H_{\frac{1}{2},t}H^{SP}_{\frac{1}{2},0} + H_{-\frac{1}{2},t}H^{SP}_{-\frac{1}{2},0}) + (H_{\frac{1}{2},0}H^T_{\frac{1}{2},+,-} + H_{\frac{1}{2},0}H^T_{\frac{1}{2},0,t} \\
&+ H_{\frac{1}{2},+}H^T_{\frac{1}{2},+,0} + H_{\frac{1}{2},+}H^T_{\frac{1}{2},+,t} + H_{-\frac{1}{2},0}H^T_{-\frac{1}{2},+,-} + H_{-\frac{1}{2},0}H^T_{-\frac{1}{2},0,t} + H_{-\frac{1}{2},-}H^T_{-\frac{1}{2},0,-} + H_{-\frac{1}{2},-}H^T_{-\frac{1}{2},-,t})],
\end{aligned}$$

$$\frac{d\Gamma^{\lambda_\tau=-1/2}}{dq^2} = \frac{8}{3}(H^2_{\frac{1}{2},+} + H^2_{\frac{1}{2},0} + H^2_{-\frac{1}{2},-} + H^2_{-\frac{1}{2},0}) + \frac{2m_l^2}{3q^2}[H^{T^2}_{\frac{1}{2},+,-} + H^{T^2}_{\frac{1}{2},0,t} + H^{T^2}_{\frac{1}{2},+,0} + H^{T^2}_{\frac{1}{2},+,t} + H^{T^2}_{-\frac{1}{2},+,-} + H^{T^2}_{-\frac{1}{2},0,t} + H^{T^2}_{-\frac{1}{2},0,-} + H^{T^2}_{-\frac{1}{2},-,t} + 2(H^T_{\frac{1}{2},+,-}H^T_{\frac{1}{2},0,t} + H^T_{\frac{1}{2},+,0}H^T_{\frac{1}{2},+,t} + H^T_{-\frac{1}{2},+,-}H^T_{-\frac{1}{2},0,t} + H^T_{-\frac{1}{2},0,-}H^T_{-\frac{1}{2},-,t})] + \frac{8m_l}{3\sqrt{q^2}}(H_{\frac{1}{2},0}H^T_{\frac{1}{2},+,-} + H_{\frac{1}{2},0}H^T_{\frac{1}{2},0,t} + H_{\frac{1}{2},+}H^T_{\frac{1}{2},+,0} + H_{\frac{1}{2},+}H^T_{\frac{1}{2},+,t} + H_{-\frac{1}{2},0}H^T_{-\frac{1}{2},+,-} + H_{-\frac{1}{2},0}H^T_{-\frac{1}{2},0,t} + H_{-\frac{1}{2},-}H^T_{-\frac{1}{2},0,-} + H_{-\frac{1}{2},-}H^T_{-\frac{1}{2},-,t}). \tag{A1}$$

APPENDIX B: FORM FACTOR RELATIONS

The relations between various form factors are given as [51,52]

$$f_0 = f_1 + \frac{q^2}{M_{B_1} - M_{B_2}} f_3, \qquad f_+ = f_1 - \frac{q^2}{M_{B_1} + M_{B_2}} f_2, \qquad f_\perp = f_1 - (M_{B_1} + M_{B_2}) f_2,$$
$$g_0 = g_1 - \frac{q^2}{M_{B_1} + M_{B_2}} g_3, \qquad g_+ = g_1 + \frac{q^2}{M_{B_1} - M_{B_2}} g_2, \qquad g_\perp = g_1 + (M_{B_1} - M_{B_2}) g_2,$$
$$h_+ = f_2^T - \frac{M_{B_1} + M_{B_2}}{q^2} f_1^T, \qquad h_\perp = f_2^T - \frac{1}{M_{B_1} + M_{B_2}} f_1^T,$$
$$\tilde{h}_+ = g_2^T + \frac{M_{B_1} - M_{B_2}}{q^2} g_1^T, \qquad \tilde{h}_\perp = g_2^T + \frac{1}{M_{B_1} - M_{B_2}} g_1^T, \tag{B1}$$

with

$$f_2^T = f_T - f_T^S q^2, \qquad f_1^T = (f_T^V + f_T^S(M_{B_1} - M_{B_2}))q^2, \qquad f_1^T = -\frac{q^2}{M_{B_1} - M_{B_2}} f_3^T,$$
$$g_2^T = g_T - g_T^S q^2, \qquad g_1^T = (g_T^V + g_T^S(M_{B_1} + M_{B_2}))q^2, \qquad g_1^T = \frac{q^2}{M_{B_1} + M_{B_2}} g_3^T. \tag{B2}$$

[1] J. P. Lees *et al.* (*BABAR* Collaboration), Phys. Rev. Lett. **109**, 101802 (2012).
[2] J. P. Lees *et al.* (*BABAR* Collaboration), Phys. Rev. D **88**, 072012 (2013).
[3] M. Huschle *et al.* (Belle Collaboration), Phys. Rev. D **92**, 072014 (2015).
[4] A. Abdesselam *et al.* (Belle Collaboration), in *Proceedings of the 51st Rencontres de Moriond on Electroweak Interactions and Unified Theories: La Thuile, Italy, 2016* (ARISF, 2016).
[5] R. Aaij *et al.* (LHCb Collaboration), Phys. Rev. Lett. **115**, 111803 (2015); **115**, 159901(E) (2015).
[6] Y. Amhis *et al.* (Heavy Flavor Averaging Group), Eur. Phys. J. C **77**, 895 (2017); updated results and plots are available at https://hflav.web.cern.ch.
[7] R. Aaij *et al.* (LHCb Collaboration), Phys. Rev. Lett. **120**, 121801 (2018).
[8] R. Aaij *et al.* (LHCb Collaboration), Phys. Rev. Lett. **113**, 151601 (2014).
[9] R. Aaij *et al.* (LHCb Collaboration), J. High Energy Phys. 08 (2017) 055.
[10] C. Bobeth, G. Hiller, and G. Piranishvili, J. High Energy Phys. 12 (2007) 040.
[11] B. Capdevila, A. Crivellin, S. Descotes-Genon, J. Matias, and J. Virto, J. High Energy Phys. 01 (2018) 093.
[12] H. Na, C. M. Bouchard, G. P. Lepage, C. Monahan, and J. Shigemitsu (HPQCD Collaboration), Phys. Rev. D **92**, 054510 (2015); **93**, 119906(E) (2016).
[13] S. Fajfer, J. F. Kamenik, and I. Nisandzic, Phys. Rev. D **85**, 094025 (2012).
[14] S. Fajfer, J. F. Kamenik, I. Nisandzic, and J. Zupan, Phys. Rev. Lett. **109**, 161801 (2012).
[15] W.-F. Wang, Y.-Y. Fan, and Z.-J. Xiao, Chin. Phys. C **37**, 093102 (2013).
[16] M. A. Ivanov, J. G. Korner, and P. Santorelli, Phys. Rev. D **71**, 094006 (2005); **75**, 019901(E) (2007).
[17] C. Patrignani *et al.* (Particle Data Group), Chin. Phys. C **40**, 100001 (2016).

[18] R. Aaij *et al.* (LHCb Collaboration), Phys. Rev. D **85**, 032008 (2012).
[19] R. Aaij *et al.* (LHCb Collaboration), J. High Energy Phys. 08 (2014) 143.
[20] R. Aaij *et al.* (LHCb Collaboration), Nat. Phys. **11**, 743 (2015).
[21] M. Fiore, in *Proceedings Meeting of the APS Division of Particles and Fields (DPF 2015): Ann Arbor, Michigan, USA, 2015* (2015), http://www.slac.stanford.edu/econf/C150804/.
[22] Y. K. Hsiao and C. Q. Geng, Eur. Phys. J. C **77**, 714 (2017).
[23] R. M. Woloshyn, Proc. Sci., HADRON2013 (**2013**) 203.
[24] W. Wu, Master's thesis, Mississippi U., 2015, arXiv:1505.03418.
[25] S. Shivashankara, W. Wu, and A. Datta, Phys. Rev. D **91**, 115003 (2015).
[26] T. Gutsche, M. A. Ivanov, J. G. Korner, V. E. Lyubovitskij, and P. Santorelli, Phys. Rev. D **93**, 034008 (2016).
[27] T. Gutsche, M. A. Ivanov, J. G. Körner, V. E. Lyubovitskij, P. Santorelli, and N. Habyl, Phys. Rev. D **91**, 074001 (2015); **91**, 119907(E) (2015).
[28] W. Detmold, C. Lehner, and S. Meinel, Phys. Rev. D **92**, 034503 (2015).
[29] R. Dutta, Phys. Rev. D **93**, 054003 (2016).
[30] M. Pervin, W. Roberts, and S. Capstick, Phys. Rev. C **72**, 035201 (2005).
[31] R. N. Faustov and V. O. Galkin, Eur. Phys. J. C **76**, 628 (2016).
[32] A. Datta, S. Kamali, S. Meinel, and A. Rashed, J. High Energy Phys. 08 (2017) 131.
[33] X.-Q. Li, Y.-D. Yang, and X. Zhang, J. High Energy Phys. 02 (2017) 068.
[34] E. Di Salvo, F. Fontanelli, and Z. J. Ajaltouni, Int. J. Mod. Phys. A **33**, 1850169 (2018).
[35] F. U. Bernlochner, Z. Ligeti, D. J. Robinson, and W. L. Sutcliffe, Phys. Rev. Lett. **121**, 202001 (2018).
[36] T. Bhattacharya, V. Cirigliano, S. D. Cohen, A. Filipuzzi, M. Gonzalez-Alonso, M. L. Graesser, R. Gupta, and H.-W. Lin, Phys. Rev. D **85**, 054512 (2012).
[37] V. Cirigliano, J. Jenkins, and M. Gonzalez-Alonso, Nucl. Phys. **B830**, 95 (2010).
[38] P. Biancofiore, P. Colangelo, and F. De Fazio, Phys. Rev. D **87**, 074010 (2013).
[39] S. Aoki *et al.*, Eur. Phys. J. C **74**, 2890 (2014).
[40] T.-W. Chiu, T.-H. Hsieh, C.-H. Huang, and K. Ogawa (TWQCD Collaboration), Phys. Lett. B **651**, 171 (2007).
[41] A. G. Akeroyd and C.-H. Chen, Phys. Rev. D **96**, 075011 (2017).
[42] Y. Sakaki, M. Tanaka, A. Tayduganov, and R. Watanabe, Phys. Rev. D **88**, 094012 (2013).
[43] M. Tanaka and R. Watanabe, Phys. Rev. D **87**, 034028 (2013).
[44] A. Khodjamirian, T. Mannel, N. Offen, and Y. M. Wang, Phys. Rev. D **83**, 094031 (2011).
[45] C. Bourrely, I. Caprini, and L. Lellouch, Phys. Rev. D **79**, 013008 (2009); **82**, 099902(E) (2010).
[46] C. G. Boyd, B. Grinstein, and R. F. Lebed, Phys. Rev. Lett. **74**, 4603 (1995).
[47] C. G. Boyd, B. Grinstein, and R. F. Lebed, Phys. Lett. B **353**, 306 (1995).
[48] M. A. Ivanov, J. G. Körner, and C.-T. Tran, Phys. Rev. D **95**, 036021 (2017).
[49] C.-T. Tran, M. A. Ivanov, J. G. Körner, and P. Santorelli, Phys. Rev. D **97**, 054014 (2018).
[50] M. A. Ivanov, J. G. Körner, and C.-T. Tran, Phys. Rev. D **94**, 094028 (2016).
[51] T. Feldmann and M. W. Y. Yip, Phys. Rev. D **85**, 014035 (2012); **86**, 079901(E) (2012).
[52] C.-H. Chen and C. Q. Geng, Phys. Rev. D **64**, 074001 (2001).